nature reviews methods primers

https://doi.org/10.1038/s43586-024-00298-3

Primer

Check for updates

Fluorescence resonance energy transfer at the single-molecule level

Taekjip Ha[1,2,3] ✉, Jingyi Fei[4,5], Sonja Schmid[6,7], Nam Ki Lee[8], Ruben L. Gonzalez Jr[9], Sneha Paul[4,5] & Sanghun Yeou[8]

Abstract

Fluorescence resonance energy transfer (FRET) is a powerful spectroscopic method for measuring distances in the 2–8 nm range. Often, conformational changes and molecular interactions are difficult or impossible to synchronize, or too rare or transient to detect using ensemble FRET. Single-molecule FRET (smFRET) opens new opportunities to probe biomolecular conformational changes or interactions that are missing in static snapshots provided by traditional structural biology tools, as well as to measure the kinetics of these dynamics on various timescales and under physiological conditions, including inside cells. Advances in labelling technologies, combining smFRET with optical and magnetic tweezers and Bayesian inference-based and information theory-based analysis tools are revealing rich biomolecular dynamics. We also discuss the challenges and opportunities in integrating dynamics into traditionally static structural biology approaches, extending smFRET into cells and tissues, advancing technical innovations and democratizing the practice of smFRET.

Sections

[1]Program in Cellular and Molecular Medicine, Boston Children's Hospital, Boston, MA, USA. [2]Department of Pediatrics, Harvard Medical School, Boston, MA, USA. [3]Howard Hughes Medical Institute, Boston, MA, USA. [4]Department of Biochemistry and Molecular Biology, The University of Chicago, Chicago, IL, USA. [5]Institute for Biophysical Dynamics, The University of Chicago, Chicago, IL, USA. [6]Laboratory of Biophysics, Wageningen University and Research, Wageningen, The Netherlands. [7]Department of Chemistry, University of Basel, Basel, Switzerland. [8]Department of Chemistry, Seoul National University, Seoul, Republic of Korea. [9]Department of Chemistry, Columbia University, New York, NY, USA. ✉e-mail: taekjip.ha@childrens.harvard.edu

Introduction

Fluorescence resonance energy transfer (FRET) is a powerful spectroscopic method for measuring distances in the 2–8 nm range[1]. In this method, the excitation energy of the donor fluorophore is transferred to the acceptor fluorophore through an interaction between their transition dipoles, resulting in a measurable change in fluorescence of both fluorophores (Fig. 1). The donor and acceptor fluorophores together form a FRET pair. Small changes in the distance between the two sites of a biological molecule (where donor and acceptor are attached) can result in a detectable change in the efficiency of energy transfer, E (see Box 1, Eq. 1), allowing FRET to be used as a spectroscopic ruler. Changes in the E value can result from structural changes of a biomolecule, such as an enzyme performing Pacman-like movements, or relative motion between two different molecules (Fig. 1).

When molecular dynamics or interactions cannot be synchronized — a requirement for conventional kinetic analysis — or are too rare or transient to detect using ensemble FRET, single-molecule FRET (smFRET)[2–4] becomes valuable. smFRET provides unique real-time information on biological dynamics rather than only the average distance. Additionally, smFRET is less affected by incomplete labelling of the biomolecule of interest compared with ensemble FRET, where the fractions of molecules labelled with either the donor or the acceptor, as well as both, need to be determined to accurately measure distance. smFRET measurements can be designed to classify molecules based on such labelling stoichiometry so that only the molecules with the desired labelling stoichiometry can be analysed.

Structural databases primarily host static snapshots of biomolecules, obtained from ensemble-averaged X-ray crystallography or cryogenic electron microscopy data. By contrast, smFRET has the ability to reveal biomolecular conformational changes or interactions that are missing in these static snapshots, and to measure the kinetics of these dynamics on various timescales and under physiological conditions, including inside cells. smFRET is also not affected by the Brownian motion of the entire molecule, unlike other single-molecule techniques such as optical tweezers and magnetic tweezers that measure forces, although it has been combined with optical tweezers[5,6] and magnetic tweezers[7,8] to characterize the conformational dynamics of biomolecules as a function of force or torque, respectively.

The distance R between the donor and the acceptor at which the E value becomes 0.5 is known as R_0, and is given by Eq. 2 (see Box 1). The R_0 value is typically a few nanometres, determined by the refractive index n of the medium and properties of the FRET pair, including the spectral overlap integral J between the donor emission and acceptor absorption, the donor quantum yield ϕ_D and the relative orientation between the donor and acceptor's transition dipoles, called κ^2 (see Box 1, Eq. 3), often approximated to be 2/3. Typically, the intensities of the donor and acceptor in a single biomolecule are measured as a function of time, and if the distance between the donor and acceptor changes, these intensity values will fluctuate in an anti-correlated manner, accordingly. The E value is then determined as the acceptor intensity arising from FRET divided by the sum of both intensities after appropriate corrections[3,9] (see Box 1, Eq. 4). In an alternative approach, the fluorescence lifetime decay curve is measured and the E value is determined from the reduction in the donor lifetime[10] (see Box 1, Eq. 5).

In this Primer, we explain the components and layout of fluorescence microscopes used for smFRET studies, sample preparation and data collection both in vitro and in living cells, as well as popular analysis pipelines for the data collected and typical results obtained, followed by a few illustrative applications of smFRET. Multi-laboratory comparison studies are highlighted, emphasizing the need for standardizing data structures and improving reproducibility. Potential limitations such as fluorophore photochemistry, perturbation of biological activity, sampling bias and weak interactions are also presented along with workarounds. We end by looking to the future, when smFRET becomes integrated with other structural biology tools and becomes accessible to non-experts. We refer our readers to the excellent method and standardization-focused reviews cited throughout this Primer for additional details.

Experimentation

In this section, we discuss the experimental fundamentals of the smFRET method. We cover the components and arrangement of fluorescence microscopes used for smFRET studies, the process of sample preparation — including fluorophore selection (Box 2) — and data collection for both in vitro systems and living cells, with an emphasis on key information useful for designing future experiments. Our discussion is limited to two-colour smFRET because multi-colour smFRET remains challenging to implement for non-experts despite many successful applications[11–14].

Fluorescence microscopes used for smFRET

Instrumentation for smFRET experiments primarily aims to reduce the excitation volume as much as possible to minimize the background fluorescence signal and maximize the single fluorophore signal, which is commonly achieved using total internal reflection fluorescence (TIRF) microscopy or confocal fluorescence microscopy.

TIRF microscopy-based smFRET. TIRF microscopes generate an evanescent field of ~200 nm depth through total internal reflection (TIR) of the excitation laser at the interface between a quartz/silica glass surface, where target molecules are tethered, and the aqueous buffer containing the sample. This configuration selectively excites fluorophores near the surface of a quartz flow cell or silica glass coverslip within the evanescent field, minimizing background fluorescence from the surrounding solution and untargeted molecules[15]. In a typical two-colour TIRF system employing the popular cyanine 3 (Cy3) donor–Cy5 acceptor fluorophore pair, a 532 nm laser excites the donor, measuring both donor intensity and FRET-induced acceptor intensity, whereas a 633 nm laser serves as a control to directly excite the acceptor[16].

Fig. 1 | smFRET and its advantages. A, The fluorescence resonance energy transfer (FRET) process between two fluorophores serving as the energy donor (D) and acceptor (A). A simplified Jablonski diagram shows the electronic transitions underlying FRET and infrequent transitions to the triplet state T_1. **B**, The dependence of the FRET efficiency, E, on the donor–acceptor distance, R, plotted for a donor–acceptor pair with a FRET radius $R_0 = 5$ nm. **C**, When the donor (green) and acceptor (red) are far from each other, E is low and the emission is primarily from the donor. **D**, When the donor (green) and acceptor (red) are closer, E is high, with emission primarily from the acceptor. **E**, FRET efficiency versus distance for several different R_0 values. **F**, Time-resolved single-molecule FRET (smFRET) trajectories can reveal how a (bio)molecule progresses through its functional cycle (panel **Fa**). Instead of ensemble averages, the single-molecule resolution offers quantitative steady-state populations of the underlying functional states or conformations (panel **Fb**), revealing static or dynamic heterogeneity. The individual kinetic rate constants describing the functional dynamics of the studied system are accessible (panel **Fc**). Ensemble experiments can generally not determine such kinetic rate models at steady state.

The evanescent field can be generated through a prism (P-TIR) or through an objective (O-TIR)[3] (Fig. 2A). P-TIR uses a silica prism on top of a quartz flow cell to match the refractive index of the quartz. A mildly focused laser beam (focal length ~20 cm) enters the prism at a large incident angle (>68°), passes through a refractive index-matching oil and the quartz surface, and is reflected at the quartz–buffer interface, and a water-immersion objective lens with a long working distance and high numerical aperture (1.2) collects the fluorescence emission signals. O-TIR uses an objective lens with a high numerical aperture (>1.45) to generate an evanescent field[17]. An expanded laser beam is

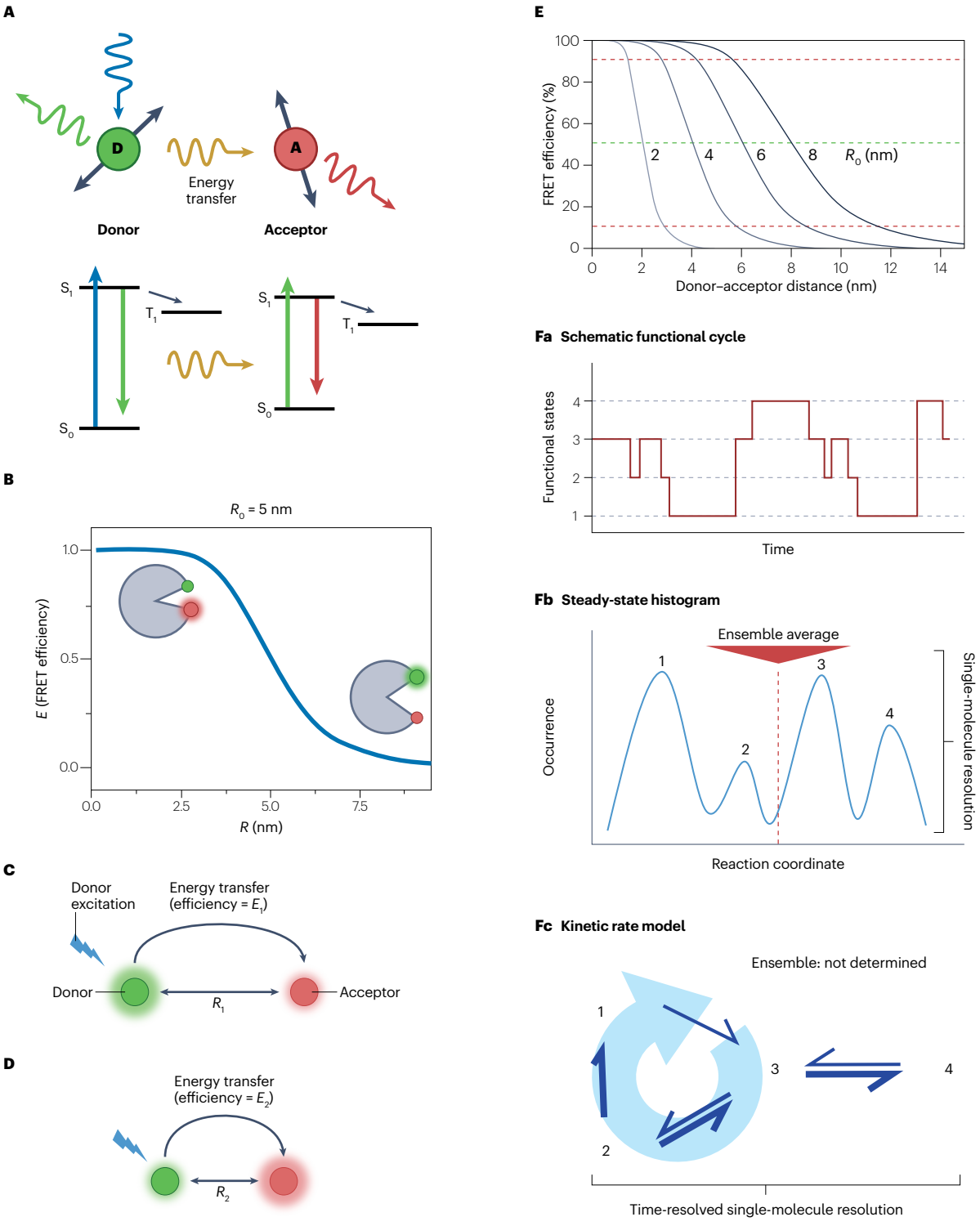

Box 1

Equations for FRET and single-molecule FRET corrections

Fluorescence resonance energy transfer (FRET) efficiency:

$$E = \frac{1}{1 + (R^6/R_0^6)} \quad (1)$$

where R is the distance between the donor and the acceptor; and R_0 is the donor–acceptor distance R at which E is 0.5.

$$\text{FRET distance [Å]}: R_0 = 0.2108 \sqrt[6]{\left(\frac{\Phi_D \kappa^2}{n^4}\right) J\,(\text{M}^{-1}\,\text{cm}^{-1}\,\text{nm}^4)} \quad (2)$$

$$\text{where } J = \int_0^\infty F_D \varepsilon_A \lambda^4 \, d\lambda$$

where Φ_D is the donor quantum yield; κ^2 is the relative orientation between the donor and acceptor's transition dipoles; n is the refractive index; J is the spectral overlap integral; F_D is the normalized donor emission spectrum; ε_A is the acceptor molar extinction coefficient; and λ is the excitation wavelength.

$$\text{Dipole orientation factor}: \kappa^2 = (\cos\theta_{AD} - 3\cos\theta_D \cos\theta_A)^2 \quad (3)$$

where θ_{AD} is the angle between the donor emission transition dipole and the acceptor absorption transition dipole; θ_D is the angle between the donor emission dipole and the vector joining the donor and acceptor; and θ_A is the angle between the acceptor absorption transition dipole and the vector joining the donor and acceptor.

$$\text{Intensity-based FRET efficiency}: E = \frac{F_{A|D}}{F_{A|D} + F_{D|D}} \quad (4)$$

where $F_{A|D}$ is the sensitized acceptor signal after donor excitation; and $F_{D|D}$ is the donor signal after donor excitation.

$$\text{Lifetime-based FRET efficiency}: E = 1 - \left(\frac{\tau_{D(A)}}{\tau_{D(0)}}\right) \quad (5)$$

where $\tau_{D(A)}$ is the donor lifetime in the presence of an acceptor; and $\tau_{D(0)}$ is the donor lifetime in the absence of an acceptor.

$$\text{Background-subtracted intensity}: I^i_{A|D} = I_{A|D} - I^{BG}_{A|D},\ I^i_{D|D} = I_{D|D} - I^{BG}_{D|D} \quad (6)$$

where $I^i_{A|D}$, $I^i_{D|D}$ is the acceptor and donor intensity with donor excitation after background subtraction, respectively; $I_{A|D}$, $I_{D|D}$ is the acceptor and donor intensity with donor excitation before background subtraction, respectively (that is, raw intensity extracted from the time-lapse images); and $I^{BG}_{A|D}$, $I^{BG}_{D|D}$ is the background signal in the acceptor and donor channels, respectively, with donor excitation (that is, signal levels after fluorophores photobleach).

$$\text{Donor emission bleed-through factor}: \alpha = \frac{I^{i(DO)}_{A|D}}{I^{i(DO)}_{D|D}} = \frac{E^{i(DO)}_{app}}{1 - E^{i(DO)}_{app}} \quad (7)$$

where $I^{i(DO)}_{A|D}$, $I^{i(DO)}_{D|D}$ is the intensity in the acceptor and donor channel, respectively, from a donor-only sample with donor excitation; and $E^{i(DO)}_{app}$ is the apparent FRET efficiency of a donor-only sample.

$$\text{Acceptor direct excitation correction factor}: \delta = \frac{I^{i(AO)}_{A|D}}{I^{i(AO)}_{A|A}} = \frac{S^{i(AO)}_{app}}{1 - S^{i(AO)}_{app}} \quad (8)$$

where $I^{i(AO)}_{A|D}$, $I^{i(AO)}_{A|A}$ is the intensity in the acceptor and donor channel using and donor and acceptor, respectively, from an acceptor-only sample; and $S^{i(AO)}_{app}$ is the apparent stoichiometry of an acceptor-only sample. Stoichiometry, S, is defined in Eq. 12 below.

$$F_{A|D} \text{ signal after } \alpha \text{ and } \delta \text{ correction}: F_{A|D} = I^i_{A|D} - \alpha I^i_{D|D} - \delta I^i_{A|A} \quad (9)$$

where $F_{A|D}$ is the fluorescence signal of acceptor with donor excitation after correction with α and δ factors; $I^i_{A|D}$, $I^i_{D|D}$ is the background-subtracted acceptor and donor intensity using donor excitation, respectively; and $I^i_{A|A}$ is the background-subtracted acceptor intensity using acceptor excitation.

$$\gamma \text{ factor}: \gamma = \frac{\eta_A \Phi_A}{\eta_D \Phi_D} \quad (10)$$

where η_A is the acceptor detection efficiency; η_D is the donor detection efficiency; and Φ_A is the acceptor quantum yield.

$$F_{D|D} \text{ signal after } \gamma\text{-factor correction}: F_{D|D} = \gamma I^i_{D|D} \quad (11)$$

where $F_{D|D}$ is the fluorescence signal of the donor with donor excitation after correction with the γ factor; and $I^i_{D|D}$ is the background-subtracted donor intensity using donor excitation.

$$\text{Stoichiometry}: S = \frac{F_{A|D} + F_{D|D}}{F_{A|D} + F_{D|D} + F_{A|A}} \quad (12)$$

$$\beta \text{ factor}: \beta = \frac{\sigma_A I_A}{\sigma_D I_D} \quad (13)$$

where σ_A is the acceptor absorption cross-section; σ_D is the donor absorption cross-section; I_A is the acceptor excitation intensity; and I_D is the donor excitation intensity.

$$\text{Determination of } \gamma \text{ and } \beta: \frac{1}{S} = (1 - \gamma)\beta E + \gamma\beta + 1 \quad (14)$$

$$F_{A|A} \text{ signal after } \beta\text{-factor correction}: F_{A|A} = \frac{1}{\beta} I^i_{A|A} \quad (15)$$

where $F_{A|A}$ is the fluorescence signal of acceptor with acceptor excitation after correction with the β factor; and $I^i_{A|A}$ is the background-subtracted acceptor intensity using acceptor excitation.

focused at the back focal plane of the objective lens, and then exits through the periphery of the objective lens to produce an evanescent field at the quartz/silica glass–buffer interface. Notably, the autofluorescence arising from the laser beam going through the objective lens in O-TIR may induce higher background signals in the red channel than is seen with P-TIR[18]. P-TIR typically has a wider field of view but requires more frequent realignment and the prism limits access to the flow cell from above, thereby impeding the incorporation of additional tools.

Fluorescence emission signals from the donor and acceptor are split by a dichroic mirror[3]. For example, for the commonly used Cy3–Cy5 pair, a high-pass optical filter with a 550 nm cut-off is placed ahead of a high-pass dichroic mirror with a 640–650 nm cut-off to separate Cy3 and Cy5 signals into two separate light paths. Band-pass optical filters mounted on the Cy3 and Cy5 light paths, respectively, are then used to remove scattered excitation light and any background signals. Each light path is then either aligned to form an image on an electron multiplying charge-coupled device (EMCCD) or a scientific complementary metal oxide semiconductor (sCMOS) camera[19]. EMCCDs have been prevalent due to their high photon detection efficiencies with minimal background, but recent advancements in sCMOS quantum efficiency has enabled single-photon detection, offering an alternative with higher time resolution for investigating fast dynamics.

Confocal microscopy-based smFRET. In a confocal microscope[16,20], the excitation beam is focused to a diffraction-limited spot using an objective lens, and emissions from the excited fluorophores are collected through the same objective lens (Fig. 2B). The emitted light from a confocal volume of approximately 1 fl is then imaged onto a 100 µm pinhole that transmits the emission signals and rejects out-of-focus background, ensuring easy alignment and a sufficient signal-to-noise ratio for smFRET[21]. After passing through the pinhole, emission signals are separated into two pathways by a dichroic mirror and re-focused onto two single-photon detectors, such as photon-counting silicon avalanche photodiodes (APDs) and hybrid photodetectors[22].

To obtain accurate smFRET data and fluorophore labelling status, two continuous laser excitations for the donor and the acceptor are alternated using electro-optic modulators[21] or acousto-optic modulators[23] with alternating periods of 50–100 µs. An analogue output device anti-synchronizes the excitation periods of the two lasers using the modulators. The emission photons are then detected by APDs, with arrival times recorded with a counter/timer device. This alternating laser excitation (ALEX) mode can also be achieved by using pulsed-interleaved excitation or enhanced using nanosecond ALEX, where the two pulsed lasers operate at frequencies of 1–50 MHz (refs. 24,25). Pulsed-interleaved excitation and nanosecond ALEX offer lifetime information in addition to the data from continuous laser ALEX mode.

Confocal microscopes can measure smFRET from both freely diffusing and surface-tethered molecules. For observing freely diffusing molecules, the excitation beam's focal point is placed 10–30 µm above the coverslip[20]. With conventional APDs, laser powers resulting in 20–30 detected photons per millisecond are sufficient to determine the average E value from thousands of single-molecule bursts. The laser typically operates at power levels ranging from 20 to 120 µW, with measurements taken prior to entering the objective lens. An optimal sample concentration of 50–100 pM allows recording of thousands of single molecules in a 10-min acquisition. High photon-counting rate measurements, which typically use surface-tethered molecules, provide temporal resolutions of tens of microseconds and are used to observe fast dynamics such as protein folding[26]. Measurements using freely diffusing molecules are suited for observing the subpopulations caused by the conformational heterogeneity and interactions of biomolecules. ALEX is crucial for confocal-based smFRET of freely diffusing molecules, providing the labelling stoichiometry information that is otherwise difficult to obtain[21].

Fluorescence microscopy combined with optical or magnetic tweezers. For complex systems or biological processes, simultaneous probing of multiple variables enables mechanistic correlation between different physical or chemical properties. The integration of optical or magnetic tweezers with single-molecule fluorescence detection — known as fleezers — expands the range of measurable biophysical quantities and allows real-time control for mechanical manipulation[7,27] (Fig. 2C).

Fleezers are structured with both a fluorescence excitation and emission detection system as well as a bead-trapping and detection system. Beads are trapped by a high-power laser (optical tweezers) or a magnetic field (magnetic tweezers). Optical tweezers use a high-power

Box 2

Fluorophore selection

Fluorophores ideal for single-molecule fluorescence measurements should have high extinction coefficients (indicating their efficiency in light excitation) and high quantum yields (indicating efficiency of excitation in producing fluorescence emission). Popular fluorophores excel in the brightness (the number of photons collected per second under standard excitation conditions), steadiness (the constancy of fluorescence intensity in the absence of biological changes) and photostability (the number of photons detectable from a single fluorophore before photobleaching).

The brightness of the single-molecule fluorescence signal is determined by both the extinction coefficient at the excitation wavelength and the emission quantum yield. Steadiness is affected by factors such as blinking, for example through sojourns to the triplet state (T_1). Despite its low frequency, T_1 is important due to its much longer lifetime (at least 1,000×) compared with the excited singlet state, and its association with photobleaching. Photostability is dependent on the host molecule, generally being higher when fluorophores are conjugated to nucleic acids compared with proteins. For in vitro single-molecule fluorescence resonance energy transfer (smFRET), an oxygen scavenger system is used to dramatically reduce photobleaching without affecting biological activities. Therefore, the performance of fluorophores under deoxygenation condition is crucial.

In the context of smFRET, a large difference in emission wavelength between the donor and the acceptor facilitates the detection of their signals with minimal crosstalk. Finally, it is desirable to have similar quantum yields between the donor and the acceptor so that FRET changes can be detected through clearly anti-correlated fluctuations in donor and acceptor intensities.

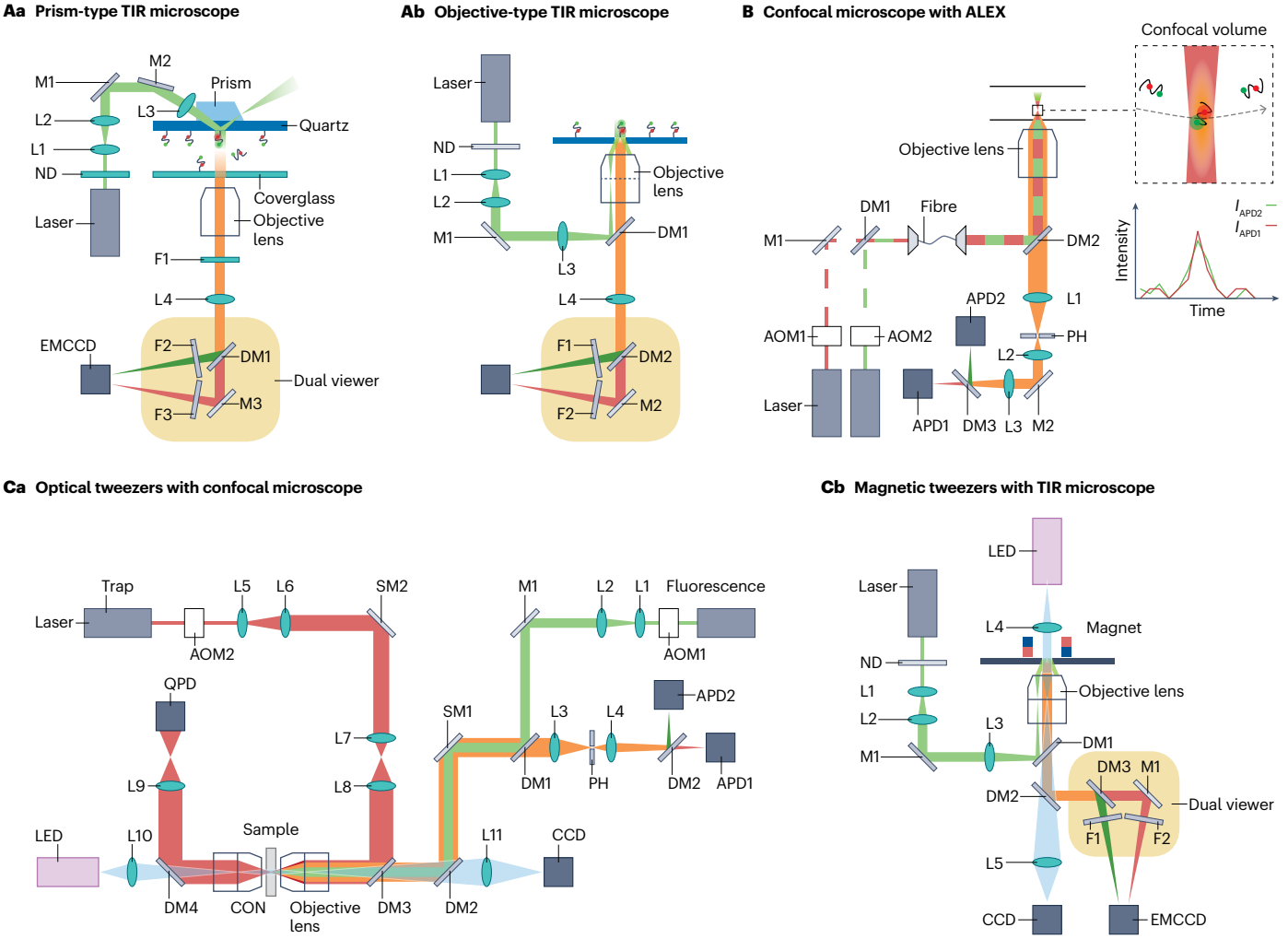

Fig. 2 | Illustration of the experimental set-ups for smFRET. A, Two types of total internal reflection (TIR) microscopes are used for observing single-molecule fluorescence resonance energy transfer (smFRET) of samples immobilized on the surface: a prism-type TIR microscope (P-TIR; panel **Aa**) and an objective-type TIR microscope (O-TIR; panel **Ab**). **B**, A confocal microscope is typically used for observing smFRET of freely diffusing molecules or immobilized molecules with a high photon counting rate. With alternating laser excitation (ALEX), the acceptor is directly excited with a red laser when the donor excitation laser is off so that the labelling stoichiometry can be determined. **C**, Typical set-ups for smFRET combined with optical tweezers (panel **Ca**) and magnetic tweezers (panel **Cb**). Red denotes the acceptor or its signal and green denotes the donor or its signal. AOM1–AOM2, acoustic optical modulators 1–2; APD1–APD2, avalanche photodiodes 1–2; CON, condenser; DM1–DM4, dichroic mirrors 1–4; EMCCD, electron multiplying charge-coupled device; F1–F4, filters 1–4; L1–L11, lenses 1–11; M1–M3, mirrors 1–3; ND, neutral density filter; PH, pinhole; QPD, quadrant photodiode; SM1–SM2, steerable mirrors 1–2.

(>1 W) near-infrared laser focused using a high numerical aperture (1.2–1.4) objective lens, with a position-sensitive detector monitoring the displacement and force applied to the trapped bead.

Fluorescence microscopes for live-cell smFRET. To observe smFRET in a living cell[28–31], several additional components need to be added to the smFRET microscopes described above. These include a motorized stage to automatically select the region of interest, a stage incubator that maintains temperature and CO_2 levels to keep cells alive and a non-fluorescence-based imaging component for observing cell morphology, such as differential interference contrast imaging or phase contrast imaging component. Most smFRET studies in eukaryotic cells have been performed on membrane proteins and their ligands[28,32] because measuring smFRET in the 3D space of eukaryotic cytosols still remains challenging[33].

Sample preparation

Fluorophore labelling of biomolecules. Fluorophores with a high extinction coefficient (>50,000 M^{-1} cm^{-1}) and reasonable quantum yield (>0.1) can be used for smFRET[3,16]. Fluorescent proteins (FPs) need no additional post-cloning steps for conjugation with the target protein. Quantum dots, being highly resistant to photobleaching, may enable prolonged FRET observation. In vitro smFRET experiments have employed FPs and quantum dots[34,35], although they have several disadvantages that have precluded practical applications. FPs have a large size and low photostability relative to organic fluorophores, and

quantum dots, with an even larger size and broader absorption spectra, face practical limitations. Consequently, organic fluorophores are more commonly used for smFRET experiments. Organic fluorophores with absorption wavelengths of 480–600 nm (such as Cy3, Cy3B, Alexa Fluor (AF) 488, AF555, ATTO488, ATTO532, LD550 and LD555) are commonly used as donors, whereas those with absorption wavelengths of 600–700 nm (such as Cy5, ATTO647N, AF594, AF647, LD650 and LD655) are used as acceptors. Notably, the Cy3–Cy5 and AF488–AF594 FRET pairs are frequently employed. Multi-colour smFRET is useful for observing multiple distances within a molecule and interactions among more than two components. However, the available number of fluorophores is constrained by spectral overlaps between dyes. Commonly used fluorophore combinations for multi-colour smFRET are Cy3/Cy5/Cy5.5 (ref. 11) or Cy3/Cy5/Cy7 (ref. 36) for three-colour smFRET and Cy2/Cy3/Cy5/Cy7, Alexa488/Cy3/Cy5/Cy7 (ref. 13) or Atto488/Atto550/Atto594/Atto647N (ref. 37) for four-colour smFRET.

For labelling biomolecules of interest, fluorophores functionalized with chemically reactive groups such as *N*-hydroxysuccinimide (NHS) esters and maleimides are used. NHS esters label amine-modified nucleic acids or lysine residues in proteins. Maleimide-functionalized fluorophores allow site-specific labelling of proteins, by reacting with thiol-modified nucleic acids or cysteine residues. After labelling, checking labelling efficiency through purification steps is crucial, but smFRET's advantage lies in reduced dependency on high labelling efficiency, as fluorescence signals provide information on each molecule's labelling status. Finally, unnatural amino acid mutagenesis is increasingly applied to introduce a single unnatural amino acid amenable to labelling via biorthogonal chemistry[38–41].

Surface tethering of biomolecules. In TIRF microscopy-based smFRET, preventing non-specific adsorption of molecules to the quartz/silica glass surface is critical. This is achieved by passivating the surface with a mixture of NHS-functionalized, biotinylated and non-biotinylated polyethylene glycol (PEG) grafted onto the aminopropyl silane-functionalized quartz/silica glass surface[3]. Streptavidin doping allows tethering of a biotinylated biomolecule of interest to the surface using a biotin–streptavidin–biotin bridge. We refer the interested readers to an illustrated protocol on how the same chamber is created and functionalized[42]. Although surface preparation is time-consuming and each surface is generally used only once, new protocols offer regeneration of PEG surfaces up to ten times without quality loss, promising increased throughput and cost reduction[43]. An alternative approach involves using dichlorodimethylsilane and Tween-20, which efficiently prevented non-specific adsorption of biomolecules to a streptavidin-coated surface[44]. Additionally, encapsulating freely diffusing biomolecules in liposomes[45] and employing anti-Brownian electrokinetic traps[46] provide alternatives to direct tethering to the surface.

Preparation of fluorophore-labelled samples for live-cell smFRET. smFRET in living cells can be performed with a genetically encoded FRET pair, either of FPs or organic fluorophores linked to genetic tags such as SNAP-Tag, CLIP-tag and HaloTag[31]. Use of FPs and genetic tags is limited by their large size and the restricted positions where they can be introduced[47,48]. To address these drawbacks, labelled biomolecules can be exogenously introduced into live cells, employing methods such as microinjection in the case of eukaryotic cells[28,49] or transformation approaches such as heat shock or electroporation for bacterial cells[29,30].

Reducing cellular autofluorescence is crucial for live-cell smFRET. In eukaryotic cell lines, avoiding common supplements to culture media such as phenol red is essential, as they can generate artificial signals[17]. For bacterial cells, live-cell imaging typically employs minimal media such as 3-(*N*-morpholino)propanesulfonic acid (MOPS) and M9, instead of Luria–Bertani medium which has a high background fluorescence signal[50,51].

Data collection

Time-series data from surface-tethered biomolecules. Time-series data are generated by recording the fluorescence emission signals from fluorophore-labelled, surface-tethered biomolecules over time. Commercial (MetaMorph from Molecular Devices), open-source (μManager[52]) or laboratory-developed (Single[53] or smCamera) software is used to control the detectors and record the time-series data. To extend intensity and *E* trajectories, the use of an oxygen scavenging system is crucial in most systems to mitigate photobleaching. Currently, glucose oxidase with catalase (GOC) or protocatechuic 3,4-dioxygenase (PCD) with protocatechuic acid (PCA)[54] serve as oxygen scavenging agents. This system also prevents the photoinduced conversion of Cy5 into Cy3 (or photoblueing)[17,55]. Triplet-state quenchers are additionally used to reduce the triplet-state lifetime[56].

Collecting fluorescence emission bursts from freely diffusing biomolecules. Confocal microscopy is applied to observe smFRET in freely diffusing, fluorophore-labelled biomolecules, eliminating the need for surface tethering[20]. Triplet-state quenchers are used to mitigate triplet-state blinking which may occur over a timescale similar to the time a molecule spends in the excitation volume. The transit time of biomolecules

Glossary

Dwell times
Durations of time that single molecules spend in a specific fluorescence resonance energy transfer (FRET) state before transitioning to a different FRET state or photobleaching.

Excitation volume
The spatial region of the excitation laser around an imaged object in which impurities and background fluorophores may also be excited.

FRET states
Compositional or conformational states of a biomolecule that are distinguished by their fluorescence resonance energy transfer (FRET) efficiencies.

Multi-colour smFRET
Single-molecule fluorescence resonance energy transfer (smFRET) using three or more fluorophores with distinct emission colours, allowing the simultaneous monitoring of multiple energy transfer events.

Photobleaching
A photochemical reaction between the excited electronic state of a fluorophore and molecular oxygen (O_2) that destroys the fluorophore and manifests as a single-step decrease in the emission signal of a single fluorophore to the background level.

Photon budgets
The number of photons detected from a single fluorophore until photobleaching.

Triplet-state blinking
Turning off and on of a single fluorophore caused by transitions to and from a triplet electronic state, respectively.

Two-colour smFRET
The most common implementation of single-molecule fluorescence resonance energy transfer (smFRET), involving a single donor and a single acceptor fluorophore of distinct emission colours.

passing through the confocal excitation volume of ~1 fl is approximately 1 ms. Therefore, binning times of 0.5–1 ms are typically used for intensity trajectories, aiding in the selection of single-molecule bursts. Various commercial set-up solutions exist for measuring confocal smFRET with or without time-correlated single-photon counting[57].

Live-cell smFRET. Live-cell smFRET follows procedures similar to in vitro smFRET, but autofluorescence presents an additional challenge. Autofluorescence in this context varies depending on the cells and fluorescence detection method. Lifetime-based fluorescence measurements offer more accurate values of E for live cells, because autofluorescence has specific (shorter) lifetimes in the cells, and thus it can be corrected for[29].

Results

In this section, we describe the typical analysis pipelines for the data collected from the two most common smFRET instruments — TIRF and confocal fluorescence microscopes — and we discuss the typical results obtained from each set-up.

TIRF-based smFRET

With TIRF-based smFRET, raw data consist of movies with separate donor and acceptor images recorded over time (Fig. 3a). Image processing outputs the extracted intensity trajectories for each donor–acceptor pair (Fig. 3b), which can be converted to E trajectories using Eq. 4 (Box 1). Major processing steps involve image alignment, fluorophore identification and trajectory selection. In image alignment, the donor and acceptor images are spatially mapped. Markers that emit in both channels (such as TetraSpeck Fluorescent Microspheres from ThermoFisher) can be recorded as calibration data, and the spatial correction parameters (x and y shifts, rotation, expansion and distortion) are then obtained by polynomial fitting of the marker images[16]. In fluorophore identification, fluorescence spots are detected using a spot detection algorithm with user-defined thresholds. An optimal background subtraction often improves the accuracy of fluorescent intensity calculation[58]. Commercial and open-source software (such as ImageJ) typically contain built-in features for spot detection[59]. Spots from the donor images are mapped onto the acceptor images or vice versa. In trajectory selection, intensity trajectories arising from more than one fluorophore with low signal-to-noise ratio or of low quality due to factors such as drift are discarded at this step. Many laboratory-developed open-source software packages such as MASH-FRET[60], SPARTAN[19], TwoTone[61], iSMS[62] DeepFRET[63], AutoSiM[64], MARS[65] and Deep-LASI[66] are employed for these image processing and trajectory selection steps, increasingly in semi-automated or fully automated procedures. A detailed description of the software packages is summarized in a recent review article[16].

Correction of intensity trajectories. Intensity trajectories undergo correction for several instrument and fluorophore properties[9] (Fig. 3c–e). Background subtraction for both donor and acceptor intensities using Eq. 6 (Box 1) ensures an average intensity value of zero after photobleaching. The donor emission bleed-through correction factor (α) is determined using Eq. 7 (Box 1). This step requires a sample with a donor-only label, or a time window after acceptor photobleaching in individual trajectories (Fig. 3c). The acceptor direct excitation correction factor (δ) is determined using Eq. 8 (Box 1). This step typically requires a sample with an acceptor-only label, or a time window after donor photobleaching in individual trajectories (Fig. 3d). Application of Eq. 9 (Box 1) can correct the acceptor signal for donor emission bleed-through into the acceptor channel and direct excitation of the acceptor at the donor excitation wavelength. After these three corrections, the donor-only population should have an average E value of zero. The γ factor accounts for the difference between the donor and acceptor quantum yields and detection efficiencies (see Box 1, Eq. 10) estimated from intensity trajectories as the ratio of the decrease in acceptor signal and the increase in the donor signal after acceptor photobleaches[67] (Fig. 3e). Applying Eq. 11 (Box 1) corrects the donor signal for the γ factor. Corrected donor and acceptor intensity trajectories are used to calculate E trajectories according to Eq. 4 (Box 1). These corrections eliminate experimental offsets and distortions from the data, enhancing reproducibility and accurate E values for absolute inter-fluorophore distances, crucial in structural studies. Flexible linkers necessitate averaged E values for Eq. 1 (Box 1). For a more accurate extraction of inter-fluorophore distances, various dye models are developed to account for the translational and rotational flexibility of the fluorophores (reviewed in refs. 10,16,68). In many applications, a dye model where dye rotation and dye translation occur much faster and slower than the FRET process, respectively, is appropriate. Nevertheless, partial correction (with δ correction and γ correction being optional) often suffices. For example, applications in kinetics of molecular interactions and conformational dynamics do not require absolute distance calculation, and the subpopulations of biomolecules can still be reliably identified using the apparent E values after partial correction[3].

Both intensity and E trajectories contain a wealth of kinetic information on biological processes, for example how many different conformation states exist and what their dwell times are. Hidden Markov modelling[69] (Fig. 3f), most recently implemented using Bayesian inference approaches[70], is used to determine the number of distinct FRET states and their corresponding E values, as well as the rates of transitions between these states. The transition density plot is used to pictorially visualize the relative frequency of interconversion between each pair of FRET states (Fig. 3g). More recent advances allow analysis of ensembles of single-molecule time series using an empirical Bayesian inference approach[71], inference of transition rates higher than the acquisition rate of the detector[72] and lower than the inverse of the imaging time[73], determination of kinetic parameters for systems exhibiting heterogeneous kinetics[74,75] and analyses using Bayesian non-parametric approaches[76]. Software tools such as HaMMy[69], vbFRET[77], ebFRET[71], SMACKS[74] and the recently developed tMAVEN[70] aid in kinetic analysis, whereas other software packages include integrated features for image processing, trajectory selection and corrections, modelling and parameter extraction and data visualization (SPARTAN[19], DdeepFRET[63], AutoSiM[64] and tMAVEN[70]). A detailed description of the software packages is summarized in a recent review article[16].

Confocal-based smFRET

In standard smFRET experiments using a confocal fluorescence microscope, freely diffusing biomolecules are detected during their short transit time (~1 ms) through the excitation volume (~1 fl) generated by the focused laser. The signals, sampled in the microsecond time range, provide faster time resolution than TIRF-based smFRET[16], revealing rapid molecular transitions across lower energy barriers. Information in the sub-nanosecond regime can be obtained through fluorescence lifetime measurements[16,78].

Intensity-based measurements. In an intensity-based confocal smFRET experiment, donor and acceptor photon bursts are sorted

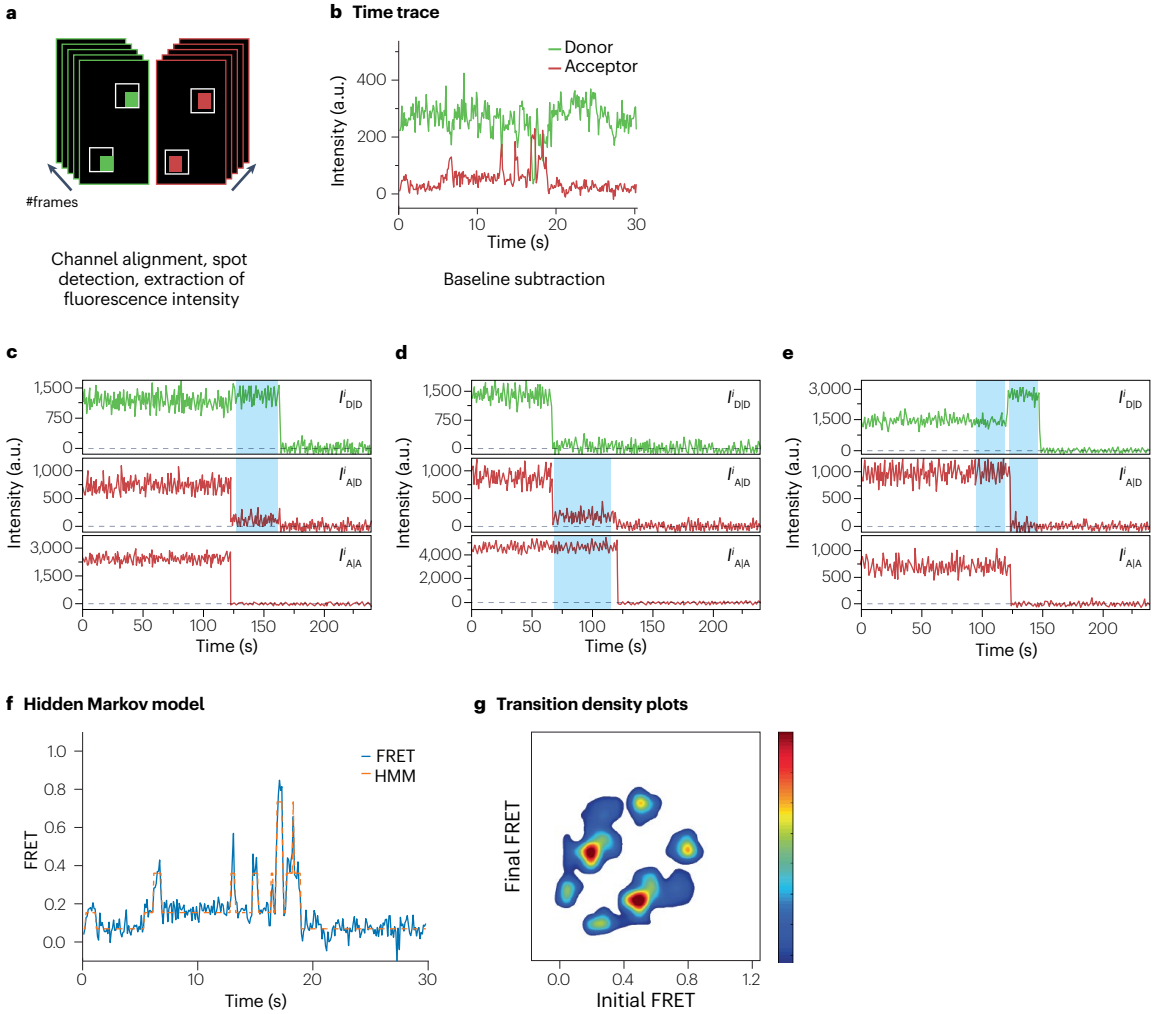

Fig. 3 | Data analysis for TIRF-based smFRET. a, Single-molecule spots in the donor (green) and acceptor (red) channels as seen in a raw total internal reflection fluorescence (TIRF) movie. **b**, Time traces are generated from the raw data. **c**–**e**, Correction factors can be estimated for individual trajectories (green lines represent donor signal, red lines represent acceptor signal). The donor emission bleed-through correction factor (α) is estimated by monitoring the residual signal in the acceptor channel after acceptor photobleaching. Traces where the acceptor photobleaches first are used (highlighted in blue region) (panel **c**). The acceptor direct excitation correction factor (δ) is estimated as the ratio of the acceptor signal upon donor excitation after donor photobleaches to the acceptor signal upon direct acceptor excitation (highlighted in blue region) (panel **d**). The γ factor can be practically determined as the ratio of the decrease in the acceptor signal to the increase in the donor signal after the acceptor photobleaches (highlighted in blue region) (panel **e**). **f**,**g**, Hidden Markov models (HMMs, panel **f**) and transition density plots (panel **g**) are often used to extract kinetic parameters from fluorescence resonance energy transfer (FRET) traces. $I^i_{A|D}$, $I^i_{D|D}$, background-subtracted acceptor and donor intensity using donor excitation, respectively; $I^i_{A|A}$, background-subtracted acceptor intensity using acceptor excitation; smFRET, single-molecule FRET. Parts **b**, **f** and **g** adapted from ref. 206, CC BY 4.0. Parts **c**–**e** adapted with permission from ref. 207, RSC.

into time bins to generate intensity trajectories (Fig. 4). Optimal binning time is estimated from the autocorrelation curves of the donor and acceptor. Background is distinguished from fluorescence emission photon bursts via intensity thresholds[23,79,80]. For instance, Symphotime analysis software (PicoQuant) allows setting intensity thresholds based on count rate histograms. Additional optional filtering steps follow event identification using properties such as burst size, burst duration and brightness.

Lifetime-based measurements. Lifetime-based smFRET is performed by recording photon arrival times with a time-correlated single-photon counting spectrometer unit coupled to the confocal microscope. The E value is calculated by the decrease in the donor lifetime in the presence of the acceptor ($\tau_{D(A)}$) relative to the donor lifetime in the absence of the acceptor ($\tau_{D(0)}$) using Eq. 5 (Box 1). Lifetime-based smFRET has advantages as certain correction factors are not required[16]. Performing both intensity-based and lifetime-based measurements ensures data consistency[81]. This approach has been used to estimate protein–protein interactions in cells[82,83], distinguish interacting and non-interacting fractions of biomolecules[84] and monitor the activity of biosensors to quantify biochemical dynamics in living cells[85,86].

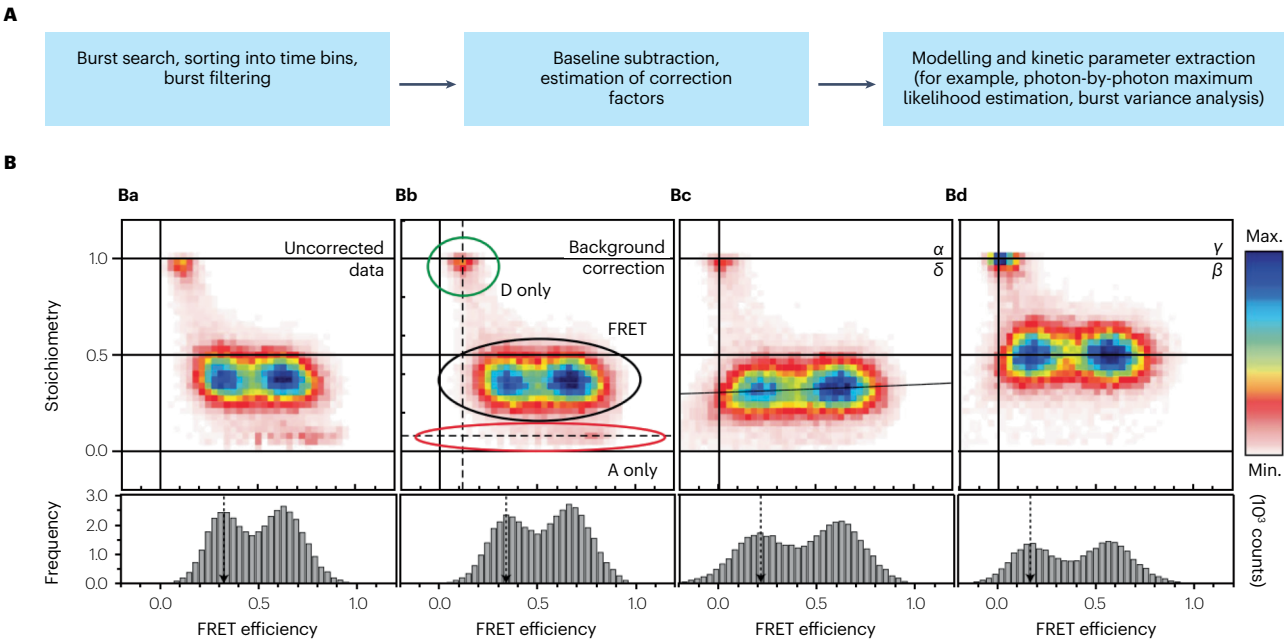

Fig. 4 | Data analysis for confocal-based smFRET. A, The process of data analysis. Photon bursts from the donor and acceptor are sorted into time bins and filtered. Threshold-based criteria can be used to distinguish bursts from background. Raw data undergo the same processing steps including background subtraction and corrections for instrument and fluorophore properties. Fast dynamics can be calculated from the confocal fluorescence resonance energy transfer (FRET) data using methods such as photon-by-photon maximum likelihood estimation and burst variance analysis. **B**, Stepwise data correction using alternating laser excitation (ALEX) (on a confocal set-up as an example) and represented as stoichiometry (S) versus FRET efficiency (E) 2D histogram. After background subtraction (panel **Ba**), from the S versus E histogram, donor emission leakage correction factor α is determined by apparent E of the donor-only population (panel **Bb**). After correction, this population should be centred at $S = 1$, $E = 0$ (panel **Bc**). The acceptor direction excitation correction factor δ is determined by S of the acceptor-only population (panel **Bb**). After correction, this population should be centred at $S = 0$ (panel **Bc**). The γ factor is corrected together with the β factor by fitting S versus FRET from different populations using Eq. 14 (Box 1) to generate the fully corrected S and E values (panel **Bd**). A, acceptor; D, donor; E, FRET efficiency; smFRET, single-molecule FRET. Part **B** reprinted from ref. 9, Springer Nature Limited.

Dynamic information extraction. Dynamic information of various biomolecules can also be extracted from the analysis of the bursts using statistical methods such as burst variance analysis[87] (Fig. 4A), the kernel density distribution estimator[88] or generating 2D histograms of E versus donor fluorescence lifetime[16,81,89]. Fast kinetics are determined through broadening of the E distribution by dynamic exchange between conformational states[90]. Photon-by-photon maximum likelihood analysis[90] and hidden Markov modelling[91,92] have facilitated the extraction of sub-millisecond to microsecond dynamics[90]. Coupling fluorescence correlation spectroscopy with smFRET estimates dynamics on timescales shorter than diffusion[93–95]. For instance, nanosecond fluorescence correlation spectroscopy has been used to probe protein folding and chain dynamics with picosecond time resolution[95]. Various available software, including Fretica[96], FRET_3colorCW (ref. 97), H²MM (ref. 91), ALiX[98], OpenSMFS[99], rFRET[100] and MFD Spectroscopy and Imaging[101], enable the semi-automated or fully automated, user-friendly analysis and extraction of kinetic parameters from confocal microscopy-based smFRET data.

ALEX and 2D analysis

In addition to yielding the E value, ALEX-based methods[21,24,102,103] offer valuable insights into the relative stoichiometry (S) (see Box 1, Eq. 12) of the FRET pair in the molecule being examined. For a molecule labelled with one donor and one acceptor, the S value is approximately 0.5, whereas it is ~1 and ~0 for a molecule with donor only and acceptor only, respectively. The results from ALEX experiments can be visually represented as E versus S heatmaps (Fig. 4B). To ensure accurate determination of the S value, an additional correction factor (β) accounting for the difference between the excitation intensity and the excitation cross-section of the donor and acceptor (see Box 1, Eq. 13) is applied. By globally fitting E and S values of all populations (see Box 1, Eq. 14), both the γ and β factors can be accurately determined. ALEX not only aids in identifying and eliminating artefacts but also distinguishes between biomolecules labelled solely with a donor (compositional heterogeneity) and those adopting conformations with large inter-fluorophore distances (conformational heterogeneity), both of which can generate apparent E values close to zero. ALEX thus provides an optimal approach for determining correction factors and accurately estimating E values[9,102] (see Box 1, Eqs. 7–15).

Applications

Most biomolecules undergo conformational fluctuations and interactions with binding partners that are crucial for their folding and/or function[104]. These fluctuations and binding interactions are stochastic and frequently difficult or impossible to synchronize, and so ensemble studies of folding and function exhibit population averaging that often complicates data analysis and interpretation. smFRET avoids such population averaging, allowing direct observations of fluctuations

and binding interactions that enable discovery and characterization of functionally critical — but rarely and/or transiently sampled — conformations and binding states. This section showcases diverse applications of smFRET and fleezers across various biological domains. We first provide a list of representative applications in each area, then delve into an exemplary application, highlighting unique insights gained through the distinctive capabilities of smFRET or fleezers.

Genome maintenance and editing

smFRET has been used to investigate the interactions of chromatin remodelling enzymes[36,105,106], DNA polymerases[107,108], DNA repair proteins[109,110] and CRISPR-associated (Cas) nucleases[111–114] with DNA or nucleosomes, and how the dynamics of these biomolecules contribute to their functions. For instance, the dynamics of the histidine–asparagine–histidine (HNH) domain of the Cas9 nuclease has been investigated using donor and acceptor fluorophores attached to the HNH domain and core of Cas9, respectively. In the absence of a guide RNA (gRNA), the HNH domain fluctuates between many positions relative to the core — an aspect of Cas9 function challenging to characterize using ensemble techniques. These fluctuations are sensitive to the binding of gRNA to Cas9 and of gRNA-programmed Cas9 to DNA, such that the HNH domain is only stably positioned into the Cas9 active site when the gRNA is properly base-paired to its DNA target, thereby activating Cas9 for DNA cleavage[112–114]. This revelation explains the mechanism underpinning the heightened accuracy of high-fidelity Cas9 variants[114] and provides a framework for the design of even more precise variants.

Gene expression and regulation

smFRET has been extensively employed to investigate various facets of gene expression and regulation, including transcription[115,116], splicing[117,118], non-coding RNA-based regulation[119,120], translation[121–123] and protein degradation[124]. Notably, studies of translation exemplify the valuable insights provided by smFRET. For example, the examination of ribosomes labelled with donor and acceptor fluorophores has unveiled dynamic fluctuations between two global conformational states that play essential roles during translation[121] (Fig. 5a). Recently, smFRET was used to directly observe these fluctuations under varying temperatures for ribosomes carrying different tRNA ligands, allowing the temperature-dependent rates of these fluctuations to be quantified[123] (Fig. 5b,c). Employing transition state theory to analyse the data enabled the enthalpic and entropic contributions to the free energy barriers governing these structural fluctuations to be determined (Fig. 5d). The findings highlight a unique role for tRNAs as entropic guides that modify the structural flexibility of the ribosome to regulate translation, in contrast to the enthalpic adjustments that ligands make to control the activities of most small protein enzyme.

Biomolecular folding and assembly

smFRET has been instrumental in unravelling intricate details of diverse biological processes, including RNA[125,126] and protein folding[26,125–127], assembly of multi-protein[128–130] and ribonucleoprotein complexes[131–134] and the contributions of chaperones in protein folding, membrane targeting and protein disaggregation[37,124,135–138]. A noteworthy instance is smFRET investigations into the trajectories proteins follow as they journey from unfolded conformations to their native conformations, trajectories known as the transition paths. Multi-colour smFRET was applied to investigate the transition paths of an intrinsically disordered protein domain — the transactivating domain (TAD) of the tumour suppressor protein p53 — during its binding to the cyclic AMP response element-binding (CREB) protein[128]. By attaching donor and acceptor (A1) fluorophores to the amino and carboxy termini of TAD, and a second acceptor (A2) fluorophore to the CREB protein, FRET from the donor fluorophore to A1 and A2 was used to directly observe folding of an individual TAD as it binds a single CREB protein. The study, leveraging the unique capability of smFRET to discern individual transition paths, revealed that CREB-mediated TAD folding follows multiple sets of paths. Notably, a relatively longer set of paths involved strong non-native electrostatic interactions, whereas several shorter sets featured weaker non-native electrostatic interactions.

Transmembrane transport and signalling

smFRET has played a crucial role in investigating the conformational dynamics of ion channels[139–141] and transporters[142–144] that drive transmembrane transport as well as those of G-protein-coupled receptors (GPCRs)[145–148] and other protein receptors[149,150] involved in transmembrane signalling. Additionally, smFRET has been used to study how protein receptor activators recognize and activate their cognate receptors[151–153].

A notable illustration of the mechanistic insights provided by smFRET comes from the investigation of the interaction between the receptor binding domain (RBD) of the Spike protein from SARS-CoV-2 and the human angiotensin converting enzyme 2 (ACE2) — a critical step for viral entry into the host cell. By attaching donor and acceptor fluorophores to the RBD and core of the Spike protein, respectively, a smFRET study revealed that the RBD fluctuates between down and up conformations. In the up conformation, the residues responsible for ACE2 receptor binding become accessible[152]. The power of smFRET lies in its ability to observe these fluctuations at the level of individual Spike proteins, avoiding the population averaging inherent to ensemble techniques. This allows quantification of transition rates between the down and up conformations and the thermodynamic stabilities of these states. Strikingly, a mutation associated with more infective SARS-CoV-2 variants was found to decrease the up-to-down transition rate and thermodynamically stabilize the up conformation, at least partially explaining the increase in this variant's infectivity[152] and providing a framework for predicting the infectivity of emergent variants.

Probing biomolecular responses to force with fleezers

Expanding on the applications of smFRET, fleezers offer an excellent approach to investigating the impact of force or torque on biomolecular interactions, dynamics, reactions or functional read-outs. An illustrative example involves the force-induced unwrapping of DNA within a nucleosome[154]. In this set-up, a pair of donor and acceptor fluorophores is attached to nucleosomal DNA, which is wrapped around a histone core. Applying an increasing pulling force to the DNA induces unwrapping, resulting in a corresponding decrease in the E value. Notably, the nucleosome exhibits increased stability under tension when a single base pair mismatch is introduced into the DNA[155]. Fleezers offer a distinct advantage over stand-alone optical or magnetic tweezers by leveraging E value measurements to unveil subtle conformational changes even when low forces prevent the measurements of such changes via mechanical means. For example, fleezers have proven valuable in examining conformational dynamics of Holliday junctions, showcasing sensitivity to even weak forces (<1 pN) and revealing an anisotropic energy landscape[5].

Reproducibility and data deposition

Over its nearly three-decade evolution, smFRET has matured as a biophysical technique. As its applications expand into complex biological systems, the need for method standardization has grown to

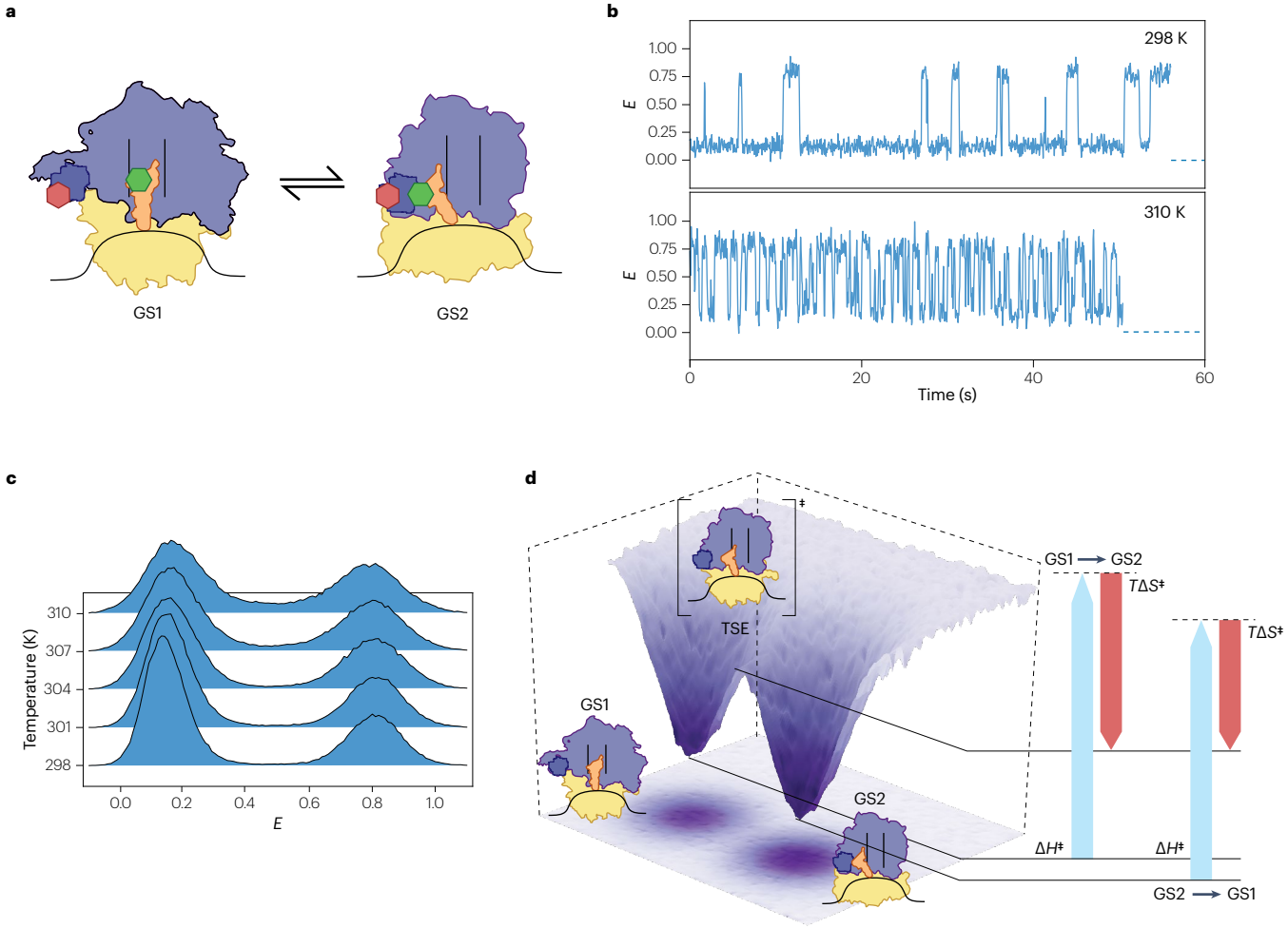

Fig. 5 | smFRET studies of the temperature dependence of ribosome conformational dynamics. a, A ribosome that has been donor (green) and acceptor (red) labelled to allow single-molecule fluorescence resonance energy transfer (smFRET) studies of a thermally driven, reversible structural rearrangement that is essential during multiple stages of translation. **b**, Representative FRET efficiency, *E*, trajectories recorded at 298 K (top) and 310 K (bottom). **c**, 1D histograms of *E* reporting on conformational transitions of the ribosome at five temperature points between 298 K and 310 K. **d**, Representation of the free energy landscape governing this structural rearrangement of the ribosome: enthalpic ($\Delta H^{\ddagger}$, blue) and entropic ($T\Delta S^{\ddagger}$, red) contributions to the free energy barriers separating two global conformational states of the ribosome (GS1 and GS2) at ~310 K. Solid lines represent the free energies of GS1 and GS2 and the transition state ensemble (TSE), whereas dotted lines represent the free energies of the TSE if the corresponding free energy barriers had been solely enthalpic in nature. Adapted with permission from ref. 123, PNAS.

ensure reproducibility, cross-evaluation and replicability. Drawing parallels with the Protein Data Bank (PDB)[156] — which is an essential data source for transformative structure prediction algorithms such as AlphaFold2 (ref. 157) — standardizing data structures emerges as a pivotal practice, fostering accessibility and advancing transformative analysis algorithms. Multiple efforts have been made to standardize data structures, including the organization of several multi-laboratory comparison studies of smFRET methods.

Multi-laboratory comparative studies

In 2012, a global initiative was launched to demonstrate the precision and accuracy of smFRET when applied in independent laboratories worldwide[9]. This initiative used fluorophore-labelled DNA samples, showcasing accurate *E* values across diverse laboratories with both TIRF-based and confocal microscopy-based smFRET. This cross-laboratory consistency was a direct result of procedure standardization, notably even without hardware standardization. The kinetic software challenge[158] scrutinized quantitative rate constant inference and uncertainties from *E* trajectories, finding that most available analysis pipelines tested could infer consistent rate constants from low-complexity data, whereas for more complicated multi-state data the results became dependent on model selection. The protein kinetics study[159] engaged 19 laboratories to validate the reproducibility of measurements of *E* values and protein conformational dynamics using confocal smFRET, further refining fluorophore models and quality criteria. These multi-laboratory studies have made standardized samples and validation data sets available for user training and evaluation of new experimental and analytical procedures[159].

Democratization of hardware is in progress, with commercially available TIRF and confocal microscopy set-ups and open-hardware projects such as the miCUBE[160] or the smfBox[161] lowering costs and technical barriers. Software standardization, however, remains a challenge. The diverse needs of individual studies often demand specialized solutions, leading to various software packages across laboratories, many of which are publicly available (see Table 1 in ref. 16). A unified, open-source software package, customizable through plug-ins, akin to super-resolution microscopy[162], would greatly benefit the smFRET field, fostering rapid dissemination of analytical tools and innovations.

Data deposition

To align with open science initiatives and funders' data-sharing requirements, routine deposition of raw data in citable open repositories is encouraged upon study publication. Public servers such as Zenodo and Figshare facilitate straightforward data deposition and management, although long-term maintenance is crucial. However, imprecise reporting of results can still impede reproducibility. The objective of reporting standards, as exemplified in Table 1, is to enhance the reproducibility and accessibility of general smFRET data. Shared data formats for raw smFRET data include, for example, Photon-HDF5 for confocal-based data and TIFF stacks for TIRF microscopy-based raw data[16]. Given the large size of TIRF data, depositing the extracted single-molecule intensity and/or *E* trajectories is computationally more efficient, convenient and sufficient for most purposes. Several condensed, text-based file formats have been proposed for this type of data[19,158,163]. Curated databases such as PDB-Dev[164] have more specific reporting requirements, hosting protein structures derived from smFRET measurements and other structural analyses that for various reasons do not meet the deposition criteria for the PDB itself.

Limitations and optimizations

Fluorophore blinking and photobleaching

Ideally, fluorophores in smFRET experiments would persist for extended periods, emitting numerous photons before photobleaching. In reality, their electronic excited state's interaction with molecular oxygen (O_2) accelerates photobleaching and limits the observation time. Enzymatic scavenging of O_2 prolongs the observation lifetime but causes longer triplet-state lifetimes[54,165], leading to triplet-state blinking (Fig. 6a). Triplet-state quenchers can mitigate triplet-state blinking (Fig. 6,c). Although effective, triplet-state quenchers can pose challenges, such as in the case of the commonly used quencher β-mercaptoethanol, whose thiol group reacts with Cy5, causing reversible blinking of Cy5. When Cy5 is in the off state due to blinking it ceases to act as an acceptor, thus increasing the donor signal as a result[165,166] (Fig. 6c). This acceptor blinking can be misinterpreted as a signature of conformational changes from processes such as protein unfolding and nucleosome DNA unwrapping. This photochemical artefact is recognizable in the apparent rate of molecular transitions, which would be dependent on the laser intensity, whereas the rates of true biomolecular transitions would not. An alternative triplet-state quencher such as Trolox can effectively eliminate triplet-state quenching (Fig. 6b) and help avoid Cy5 blinking artefacts[165,167–169] (Fig. 6d). Deuterium incorporation into fluorophores enhances photostability even without oxygen removal[170,171].

In fleezers-based smFRET experiments, some fluorophores, especially those based on carbocyanines, are rapidly photobleached when they are exposed to a trapping laser because of a two-photon absorption process[172]. This problem can be mitigated by either spatial separation[5] or temporal separation[6] of the trapping laser and the fluorescence excitation laser.

Function perturbation

The transformative insights from single-molecule measurements must not stem from measurement artefacts or modifications made during labelling, tethering or irradiation. For nucleic acid labelling, conjugating fluorophores using an amino modification on the C6 position of a thymine base is recommended because this conjugation does not perturb the backbone continuity of DNA or RNA strands. For protein labelling, a non-conserved amino acid on the surface of the protein

Table 1 | Potential reporting standards for smFRET results from TIRF or confocal experiments listed in order of increasing analysis depth

	TIRF (camera-based)	Confocal (point detector-based)
Output data	Raw movies (TIFF), extracted traces (text)[a]	Timestamped photon data (such as Photon-HDF5 and TTTR)[16]
Data set characteristics	Number of trajectories, total number of data points	For burst analysis (in solution), number of bursts and number of photons; for intensity or *E* trajectories (tethered), number of trajectories and total number of data points
Sample characteristics	Biomolecule and fluorophore attachment points; fluorophore and attachment chemistry; surface tethering approach, if applicable; additional parameters such as fluorescence anisotropy	
FRET population analysis	*E* values and their uncertainties (s.d.)[b]; populations sizes and their uncertainties (s.d.)[b]	
Distances	Distances and their uncertainties; fluorophore model and parameters used	
Kinetics	Forward/reverse rate constants (s^{-1}) and uncertainties (95% CI), criteria for model selection (BIC values or Bayesian alternatives)	For burst analysis (in solution): fluctuations, yes/no; state lifetimes and uncertainties For intensity or *E* trajectories (tethered): forward/reverse rate constants (s^{-1}) and uncertainties (95% CI), criteria for model selection (BIC values or Bayesian alternatives)

A field-wide consensus about the deposition of source data and characteristic numbers of published experiments is a hallmark of established biophysical techniques. Depositing the suggested data on single-molecule fluorescence resonance energy transfer (smFRET) experiments provides researchers with a concise and comparable summary of the results, and allows for their later re-interpretation and use in future work. BIC, Bayesian information criterion; CI, confidence interval; *E*, FRET efficiency; s.d., standard deviation; TIRF, total internal reflection fluorescence; TTTR, time tagged time-resolved fluorescence data. [a]Although TIFF stacks contain the absolute raw data, they are relatively large in file size (several gigabytes). Hence, the much smaller files of extracted traces are generally better sharable and sufficient for most purposes. [b]In intensity or *E* trajectory analysis of tethered molecules, these uncertainties are frequently dominated by heterogeneities throughout the data set; mere fitting errors (for example, from Gaussian fitting of the FRET histogram) underestimate the uncertainties involved. More accurate uncertainty measures are obtained, for example, by bootstrapping (random re-sampling with replacement). In addition, probability distribution analysis[10] can resolve time-averaging of fast dynamics, in particular, for confocal experiments with untethered molecules.

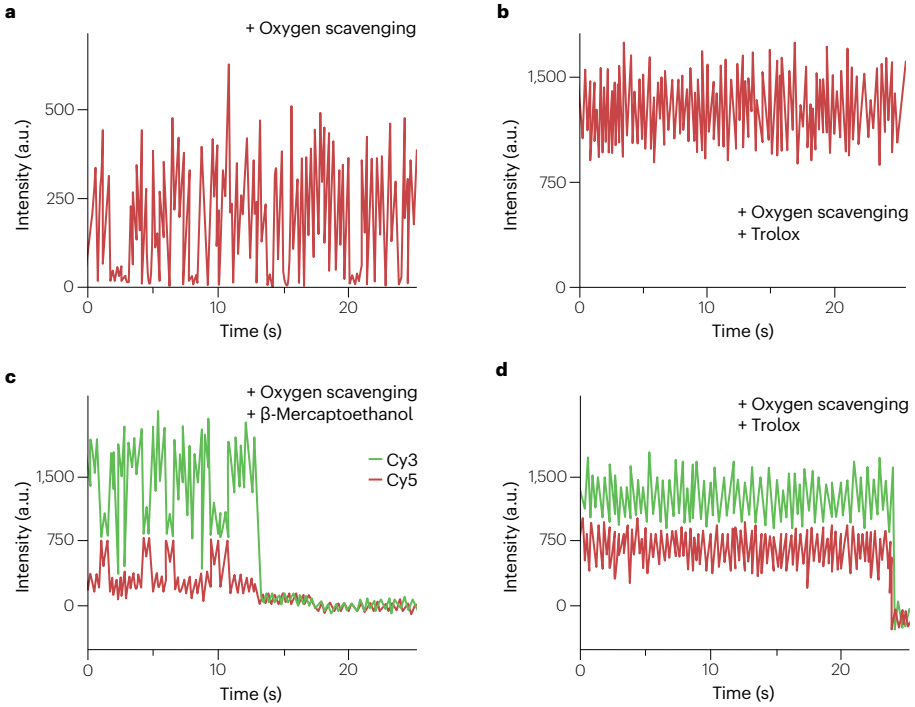

Fig. 6 | Cy5 fluorophore blinking. a, To reduce photobleaching, molecular oxygen (O_2) is enzymatically removed using oxygen scavenging. Because molecular oxygen is also an efficient quencher of the triplet state (T_1), the lifetime of the triplet state is greatly extended, causing an intermittent fluorescence signal from cyanine 5 (Cy5). **b**, Adding a triplet-state quencher such as Trolox eliminates intermittency caused by triplet-state blinking. **c**, Another triplet-state quencher, β-mercaptoethanol causes longer timescale Cy5 blinking due to reversible reaction between its thiol moiety and Cy5, giving an impression of fluorescence resonance energy transfer (FRET) changes even when there is no distance change. **d**, Trolox can avoids artefacts of Cy5 blinking, giving steady FRET signals. Reprinted from ref. 165, Springer Nature Limited.

located a distance from functionally important regions should be chosen. Recent advances in protein structure prediction[157,173] aid in choosing suitable labelling sites, even for those proteins without experimentally determined structures[173]. Functional assays post modification and after surface tethering verify activity of the labelled molecule, ensuring the reliability of the obtained information.

Sampling bias

Limitations in imaging areas, time constraints and sampling criteria can result in only a subset of molecules being recorded in typical smFRET experiments, potentially introducing bias. Prolonged imaging time may also compromise biological function, and can also lead to pH changes when using certain oxygen scavenging systems[54,174], both of which reduce the reliability of the data. Criteria for selecting appropriately labelled biomolecules may also result in biased sampling. For instance, as Cy5 is more easily photobleached than Cy3, biomolecules with a high *E* value may not survive long enough to pass a selection process, resulting in under-sampling. In kinetic analysis, heterogeneity in the rates of state transitions[125,175] means that a biomolecule with high transition rates or a biomolecule with a larger fractional occupancy of a low *E* state would contribute disproportionally more events to the dwell time histograms. Recognizing and addressing these biases, particularly in kinetic analyses, are critical for accurate determination of conformational distributions and dynamics[74,176].

Weak interactions

In traditional TIRF or confocal set-ups, high concentrations of fluorescently labelled species can impede studies of weak intermolecular interactions. Zero-mode waveguides have been used to overcome this limitation; by limiting the size of the effective excitation volume to below (50 nm)[3], on average fewer than one eighth of a single fluorophore signal will contribute to the background even at 1 µM fluorophore concentration[177]. Alternatively, molecular complexes that are transiently formed at high concentrations can be captured in a single vesicle, which can then be tethered to a surface after dilution for imaging[178].

Outlook

We see two main priorities for the smFRET field in the next 5–10 years: advancing dynamic structural biology, and expanding applications to cells, tissues and patient samples. Achieving these goals relies on robust technical innovation and democratization of the field.

Integrated and dynamic structural biology

smFRET provides 1D distance information, necessitating integrated structural modelling to leverage complementary data from techniques such as cryogenic electron microscopy, X-ray crystallography, NMR, small-angle X-ray scattering, mass spectrometry and molecular dynamics simulations. The age of dynamic structural biology has begun. Whole-protein triangulation projects have demonstrated the power of smFRET-restrained molecular dynamics simulations to describe the conformational flexibility of proteins[179,180]. Integrated smFRET-informed modelling provided substantial insights on intrinsically disordered proteins[181,182], where other techniques fail. Now, with the first smFRET-restrained protein structures deposited in PDB-Dev, the race is on to make such integrated and dynamic structural modelling the new routine for more realistic representations of biomolecules in space and time.

From cells to patient tissues

smFRET in living cells has been by recent proof-of-concept studies distinguishing protein conformations[28] and resolving conformational changes over various timescales inside live eukaryotic cells[49] or at the cell surface[32]. Extending these measurements to tissues, patient biopsy samples and living animals is a formidable but rewarding task

for the next decade. Technical challenges associated with moving forward to the clinic include portability and introduction of fluorophores into more physiological or clinical settings. An early prototype for small smFRET spectrometers that use smartphone cameras for single-molecule detection after plasmonic enhancement[183] deals with issues of portability and nanophotonic approaches break the low concentration limit, further increasing the range of biomedical applications for smFRET[184]. Generally, organic fluorophores are used for smFRET as FPs are too large and show poor photophysics. These fluorophores must be brought into cells by microinjection[28,31,49], heat shock[29] or electroporation[30], and using bio-orthogonal chemistry, fluorophores can be coupled to a biomolecule of interest even inside the cell.

Alternatively, macromolecular crowding[138] and cell lysates may be used as extracellular stepping stones en route towards more physiological conditions. In particular, cell extracts and single-molecule pull-down experiments[148,185] present an interesting option for clinical application, as they are compatible with unmodified patient samples[186]. In combination with automated multi-well plate screening[187] or sequencing chip-based high-throughput parallelization, the detection of conformational dynamics across a wide range of conditions offers a new dimension[188] of information in pharmaceutical drug screens. This additional dynamic insight provided by smFRET goes far beyond qualitative yes/no results as they provide single-molecule resolution yielding quantitative rate constants, and could therefore significantly advance medical therapy development in various areas, such as antimicrobial resistance, cancer, dementia, other neurodegenerative diseases and, in general, wherever binding or conformational dynamics play a biomedical role.

Technical innovations

As biological systems become more complex, capturing complete molecular behaviour requires increased information, often limited by photobleaching in smFRET. Ongoing research focuses on developing fluorophores with larger photon budgets and self-healing capabilities[189–191]. Photobleaching-resistant fluorophores, such as small quantum dots, nitrogen vacancy centres[192] and point defects in solid-state materials[193], may become useful in the future. Two recently described approaches, DyeCycling[194] and REFRESH-FRET[195], decouple smFRET recordings from photobleaching by using reversible fluorophore binding, breaking the photobleaching limit[196]. New (reversible) fluorophore-coupling chemistries may offer orthogonal coupling mechanisms that are fluorogenic[197], triggered by light or by buffer exchange. Unique correlative information can be obtained in combination with protein-induced fluorescence enhancement[198,199] or photoinduced electron transfer, both of which have shorter interaction radii than FRET[200]. Useful multidimensional information can also be gained from integrating smFRET with other fluorescence spectroscopy parameters (intensities, lifetimes, anisotropies or diffusivities, for instance), with sequencing[188] or with single-molecule trapping approaches[201–203]. 3D tracking[204] instead of trapping will likely find more widespread application for larger particles in solution — such as viruses — or biomolecules in viscous environments[204], including the cell[205].

Democratization and clinic-proof standards

For widespread adoption, smFRET needs improved accessibility, versatility, reproducibility and compatibility with diverse conditions, as well as enhanced standardization. Collaborative efforts between academia and private companies, similar to other advanced microscopy fields, can accelerate progress. Streamlining experiments with affordable hardware, shared protocols and open-source analysis software is imperative for achieving standardized practices, fostering acceptance and unlocking the potential of smFRET in clinical and diagnostic applications.

Published online: 28 March 2024

References

1. Stryer, L. & Haugland, R. P. Energy transfer: a spectroscopic ruler. *Proc. Natl Acad. Sci. USA* **58**, 719–726 (1967).
2. Ha, T. et al. Probing the interaction between two single molecules — fluorescence resonance energy transfer between a single donor and a single acceptor. *Proc. Natl Acad. Sci. USA* **93**, 6264–6268 (1996).
3. Roy, R., Hohng, S. & Ha, T. A practical guide to single-molecule FRET. *Nat. Methods* **5**, 507–516 (2008).
4. Lerner, E. et al. Toward dynamic structural biology: two decades of single-molecule Forster resonance energy transfer. *Science* **359**, eaan1133 (2018).
5. Hohng, S. et al. Fluorescence-force spectroscopy maps two-dimensional reaction landscape of the holliday junction. *Science* **318**, 279–283 (2007).
6. Tarsa, P. B. et al. Detecting force-induced molecular transitions with fluorescence resonant energy transfer. *Angew. Chem. Int. Ed.* **46**, 1999–2001 (2007).
7. Shroff, H. et al. Biocompatible force sensor with optical readout and dimensions of 6 nm^3. *Nano Lett.* **5**, 1509–1514 (2005).
8. Lee, M., Kim, S. H. & Hong, S. C. Minute negative superhelicity is sufficient to induce the B–Z transition in the presence of low tension. *Proc. Natl Acad. Sci. USA* **107**, 4985–4990 (2010).
9. Hellenkamp, B. et al. Precision and accuracy of single-molecule FRET measurements—a multi-laboratory benchmark study. *Nat. Methods* **15**, 669–676 (2018).
10. Kalinin, S. et al. A toolkit and benchmark study for FRET-restrained high-precision structural modeling. *Nat. Methods* **9**, 1218–1225 (2012).
11. Hohng, S., Joo, C. & Ha, T. Single-molecule three-color FRET. *Biophys. J.* **87**, 1328–1337 (2004).
12. Clamme, J. P. & Deniz, A. A. Three-color single-molecule fluorescence resonance energy transfer. *Chemphyschem* **6**, 74–77 (2005).
13. Lee, J. et al. Single-molecule four-color FRET. *Angew. Chem. Int. Ed.* **49**, 9922–9925 (2010).
14. Feng, X. A., Poyton, M. F. & Ha, T. Multicolor single-molecule FRET for DNA and RNA processes. *Curr. Opin. Struct. Biol.* **70**, 26–33 (2021).
15. Axelrod, D., Burghardt, T. P. & Thompson, N. L. Total internal reflection fluorescence. *Annu. Rev. Biophys. Bioeng.* **13**, 247–268 (1984).
16. Lerner, E. et al. FRET-based dynamic structural biology: challenges, perspectives and an appeal for open-science practices. *eLife* **10**, e60416 (2021).
17. Cho, Y., An, H. J., Kim, T., Lee, C. & Lee, N. K. Mechanism of cyanine5 to cyanine3 photoconversion and its application for high-density single-particle tracking in a living cell. *J. Am. Chem. Soc.* **143**, 14125–14135 (2021).
18. Mashanov, G. I., Tacon, D., Knight, A. E., Peckham, M. & Molloy, J. E. Visualizing single molecules inside living cells using total internal reflection fluorescence microscopy. *Methods* **29**, 142–152 (2003).
19. Juette, M. F. et al. Single-molecule imaging of non-equilibrium molecular ensembles on the millisecond timescale. *Nat. Methods* **13**, 341–344 (2016).
20. Deniz, A. A. et al. Single-pair fluorescence resonance energy transfer on freely diffusing molecules: observation of Forster distance dependence and subpopulations. *Proc. Natl Acad. Sci. USA* **96**, 3670–3675 (1999).
21. Kapanidis, A. N. et al. Fluorescence-aided molecule sorting: analysis of structure and interactions by alternating-laser excitation of single molecules. *Proc. Natl Acad. Sci. USA* **101**, 8936–8941 (2004).
22. Oikawa, H., Takahashi, T., Kamonprasertsuk, S. & Takahashi, S. Microsecond resolved single-molecule FRET time series measurements based on the line confocal optical system combined with hybrid photodetectors. *Phys. Chem. Chem Phys* **20**, 3277–3285 (2018).
23. Nir, E. et al. Shot-noise limited single-molecule FRET histograms: comparison between theory and experiments. *J. Phys. Chem. B* **110**, 22103–22124 (2006).
24. Muller, B. K., Zaychikov, E., Brauchle, C. & Lamb, D. C. Pulsed interleaved excitation. *Biophys. J.* **89**, 3508–3522 (2005).
25. Laurence, T. A., Kong, X., Jager, M. & Weiss, S. Probing structural heterogeneities and fluctuations of nucleic acids and denatured proteins. *Proc. Natl Acad. Sci. USA* **102**, 17348–17353 (2005).
26. Chung, H. S., McHale, K., Louis, J. M. & Eaton, W. A. Single-molecule fluorescence experiments determine protein folding transition path times. *Science* **335**, 981–984 (2012).
27. Hohng, S., Lee, S., Lee, J. & Jo, M. H. Maximizing information content of single-molecule FRET experiments: multi-color FRET and FRET combined with force or torque. *Chem. Soc. Rev.* **43**, 1007–1013 (2014).
28. Sakon, J. J. & Weninger, K. R. Detecting the conformation of individual proteins in live cells. *Nat. Methods* **7**, 203–205 (2010).
29. Fessl, T. et al. Towards characterization of DNA structure under physiological conditions in vivo at the single-molecule level using single-pair FRET. *Nucleic Acids Res.* **40**, e121 (2012).

30. Crawford, R. et al. Long-lived intracellular single-molecule fluorescence using electroporated molecules. *Biophys. J.* **105**, 2439–2450 (2013).
31. Sustarsic, M. & Kapanidis, A. N. Taking the ruler to the jungle: single-molecule FRET for understanding biomolecular structure and dynamics in live cells. *Curr. Opin. Struct. Biol.* **34**, 52–59 (2015).
32. Asher, W. B. et al. Single-molecule FRET imaging of GPCR dimers in living cells. *Nat. Methods* **18**, 397–405 (2021).
33. Zhao, Z. W. et al. Spatial organization of RNA polymerase II inside a mammalian cell nucleus revealed by reflected light-sheet superresolution microscopy. *Proc. Natl Acad. Sci. USA* **111**, 681–686 (2014).
34. Brasselet, S., Peterman, E. J. G., Miyawaki, A. & Moerner, W. E. Single-molecule fluorescence resonant energy transfer in calcium concentration dependent cameleon. *J. Phys. Chem. B* **104**, 3676–3682 (2000).
35. Hohng, S. & Ha, T. Single-molecule quantum-dot fluorescence resonance energy transfer. *Chemphyschem* **6**, 956–960 (2005).
36. Poyton, M. F. et al. Coordinated DNA and histone dynamics drive accurate histone H2A.Z exchange. *Sci. Adv.* **8**, eabj5509 (2022).
37. Ratzke, C., Hellenkamp, B. & Hugel, T. Four-colour FRET reveals directionality in the Hsp90 multicomponent machinery. *Nat. Commun.* **5**, 4192 (2014).
38. Das, D. K. et al. Direct visualization of the conformational dynamics of single influenza hemagglutinin trimers. *Cell* **174**, 926–937.e12 (2018).
39. Nikic, I. & Lemke, E. A. Genetic code expansion enabled site-specific dual-color protein labeling: superresolution microscopy and beyond. *Curr. Opin. Chem. Biol.* **28**, 164–173 (2015).
40. Desai, B. J. & Gonzalez, R. L. Jr Multiplexed genomic encoding of non-canonical amino acids for labeling large complexes. *Nat. Chem. Biol.* **16**, 1129–1135 (2020).
41. England, P. M. Unnatural amino acid mutagenesis: a precise tool for probing protein structure and function. *Biochemistry* **43**, 11623–11629 (2004).
42. Joo, C. & Ha, T. Single-molecule FRET with total internal reflection microscopy. *Cold Spring Harb. Protoc.* https://doi.org/10.1101/pdb.top072058 (2012).
43. Paul, T., Ha, T. & Myong, S. Regeneration of PEG slide for multiple rounds of single-molecule measurements. *Biophys. J.* **120**, 1788–1799 (2021).
44. Hua, B. et al. An improved surface passivation method for single-molecule studies. *Nat. Methods* **11**, 1233–1236 (2014).
45. Boukobza, E., Sonnenfeld, A. & Haran, G. Immobilization in surface-tethered lipid vesicles as a new tool for single biomolecule spectroscopy. *J. Phys. Chem. B* **105**, 12165–12170 (2001).
46. Cohen, A. E. & Moerner, W. E. Method for trapping and manipulating nanoscale objects in solution. *Appl. Phys. Lett.* **86**, 093109 (2005).
47. Pollok, B. A. & Heim, R. Using GFP in FRET-based applications. *Trends Cell Biol.* **9**, 57–60 (1999).
48. Bajar, B. T., Wang, E. S., Zhang, S., Lin, M. Z. & Chu, J. A guide to fluorescent protein FRET pairs. *Sensors* **16**, 1488 (2016).
49. Konig, I. et al. Single-molecule spectroscopy of protein conformational dynamics in live eukaryotic cells. *Nat. Methods* **12**, 773–779 (2015).
50. Yang, S. et al. Transcription and translation contribute to gene locus relocation to the nucleoid periphery in *E. coli*. *Nat. Commun.* **10**, 5131 (2019).
51. Stracy, M. et al. Live-cell superresolution microscopy reveals the organization of RNA polymerase in the bacterial nucleoid. *Proc. Natl Acad. Sci. USA* **112**, E4390–4399 (2015).
52. Edelstein, A. D. et al. Advanced methods of microscope control using muManager software. *J. Biol. Methods* **1**, e10 (2014).
53. Seo, M. H., Park, J., Kim, E., Hohng, S. & Kim, H. S. Protein conformational dynamics dictate the binding affinity for a ligand. *Nat. Commun.* **5**, 3724 (2014).
54. Aitken, C. E., Marshall, R. A. & Puglisi, J. D. An oxygen scavenging system for improvement of dye stability in single-molecule fluorescence experiments. *Biophys. J.* **94**, 1826–1835 (2008).
55. Helmerich, D. A., Beliu, G., Matikonda, S. S., Schnermann, M. J. & Sauer, M. Photoblueing of organic dyes can cause artifacts in super-resolution microscopy. *Nat. Methods* **18**, 253–257 (2021).
56. Zheng, Q. et al. Ultra-stable organic fluorophores for single-molecule research. *Chem. Soc. Rev.* **43**, 1044–1056 (2014).
57. Zosel, F., Mercadante, D., Nettels, D. & Schuler, B. A proline switch explains kinetic heterogeneity in a coupled folding and binding reaction. *Nat. Commun.* **9**, 3332 (2018).
58. Preus, S., Hildebrandt, L. L. & Birkedal, V. Optimal background estimators in single-molecule FRET microscopy. *Biophys. J.* **111**, 1278–1286 (2016).
59. Deschout, H. et al. Precisely and accurately localizing single emitters in fluorescence microscopy. *Nat. Methods* **11**, 253–266 (2014).
60. Borner, R. et al. Simulations of camera-based single-molecule fluorescence experiments. *PLoS ONE* **13**, e0195277 (2018).
61. Holden, S. J. et al. Defining the limits of single-molecule FRET resolution in TIRF microscopy. *Biophys. J.* **99**, 3102–3111 (2010).
62. Preus, S., Noer, S. L., Hildebrandt, L. L., Gudnason, D. & Birkedal, V. iSMS: single-molecule FRET microscopy software. *Nat. Methods* **12**, 593–594 (2015).
63. Thomsen, J. et al. DeepFRET, a software for rapid and automated single-molecule FRET data classification using deep learning. *eLife* **9**, e60404 (2020).
64. Li, J., Zhang, L., Johnson-Buck, A. & Walter, N. G. Automatic classification and segmentation of single-molecule fluorescence time traces with deep learning. *Nat. Commun.* **11**, 5833 (2020).
65. Huisjes, N. M. et al. Mars, a molecule archive suite for reproducible analysis and reporting of single-molecule properties from bioimages. *eLife* **11**, e75899 (2022).
66. Wanninger, S. et al. Deep-LASI: deep-learning assisted, single-molecule imaging analysis of multi-color DNA origami structures. *Nat. Commun.* **14**, 6564 (2023).
67. McCann, J. J., Choi, U. B., Zheng, L., Weninger, K. & Bowen, M. E. Optimizing methods to recover absolute FRET efficiency from immobilized single molecules. *Biophys. J.* **99**, 961–970 (2010).
68. Dimura, M. et al. Quantitative FRET studies and integrative modeling unravel the structure and dynamics of biomolecular systems. *Curr. Opin. Struct. Biol.* **40**, 163–185 (2016).
69. McKinney, S. A., Joo, C. & Ha, T. Analysis of single-molecule FRET trajectories using hidden Markov modeling. *Biophys. J.* **91**, 1941–1951 (2006).
70. Verma, A. R. et al. Increasing the accuracy of single-molecule data analysis using tMAVEN. *Biophys. J.* https://doi.org/10.1016/j.bpj.2024.01.022 (2024).
71. van de Meent, J. W., Bronson, J. E., Wiggins, C. H. & Gonzalez, R. L. Jr Empirical Bayes methods enable advanced population-level analyses of single-molecule FRET experiments. *Biophys. J.* **106**, 1327–1337 (2014).
72. Kinz-Thompson, C. D. & Gonzalez, R. L. Jr Increasing the time resolution of single-molecule experiments with Bayesian inference. *Biophys. J.* **114**, 289–300 (2018).
73. Kim, S. E., Lee, I. B., Hyeon, C. & Hong, S. C. Deciphering kinetic information from single-molecule FRET data that show slow transitions. *J. Phys. Chem. B* **119**, 6974–6978 (2015).
74. Schmid, S., Gotz, M. & Hugel, T. Single-molecule analysis beyond dwell times: demonstration and assessment in and out of equilibrium. *Biophys. J.* **111**, 1375–1384 (2016).
75. Hon, J. & Gonzalez, R. L. Jr Bayesian-estimated hierarchical HMMs enable robust analysis of single-molecule kinetic heterogeneity. *Biophys. J.* **116**, 1790–1802 (2019).
76. Sgouralis, I. et al. A Bayesian nonparametric approach to single molecule forster resonance energy transfer. *J. Phys. Chem. B* **123**, 675–688 (2019).
77. Bronson, J. E., Fei, J., Hofman, J. M., Gonzalez, R. L. Jr & Wiggins, C. H. Learning rates and states from biophysical time series: a Bayesian approach to model selection and single-molecule FRET data. *Biophys. J.* **97**, 3196–3205 (2009).
78. Nagl, S. et al. Microarray analysis of protein–protein interactions based on FRET using subnanosecond-resolved fluorescence lifetime imaging. *Biosens. Bioelectron.* **24**, 397–402 (2008).
79. Sisamakis, E., Valeri, A., Kalinin, S., Rothwell, P. J. & Seidel, C. A. Accurate single-molecule FRET studies using multiparameter fluorescence detection. *Methods Enzymol.* **475**, 455–514 (2010).
80. Knop, J. M., Patra, S., Harish, B., Royer, C. A. & Winter, R. The deep sea osmolyte trimethylamine *N*-oxide and macromolecular crowders rescue the antiparallel conformation of the human telomeric G-quadruplex from urea and pressure stress. *Chemistry* **24**, 14346–14351 (2018).
81. Gopich, I. V. & Szabo, A. Theory of the energy transfer efficiency and fluorescence lifetime distribution in single-molecule FRET. *Proc. Natl Acad. Sci. USA* **109**, 7747–7752 (2012).
82. Margineanu, A. et al. Screening for protein–protein interactions using Forster resonance energy transfer (FRET) and fluorescence lifetime imaging microscopy (FLIM). *Sci. Rep.* **6**, 28186 (2016).
83. George Abraham, B. et al. Fluorescent protein based FRET pairs with improved dynamic range for fluorescence lifetime measurements. *PLoS ONE* **10**, e0134436 (2015).
84. Becker, W. Fluorescence lifetime imaging—techniques and applications. *J. Microsc.* **247**, 119–136 (2012).
85. Levitt, J. A. et al. Quantitative real-time imaging of intracellular FRET biosensor dynamics using rapid multi-beam confocal FLIM. *Sci. Rep.* **10**, 5146 (2020).
86. Reissaus, C. A. et al. PIE-FLIM measurements of two different FRET-based biosensor activities in the same living cells. *Biophys. J.* **118**, 1820–1829 (2020).
87. Torella, J. P., Holden, S. J., Santoso, Y., Hohlbein, J. & Kapanidis, A. N. Identifying molecular dynamics in single-molecule FRET experiments with burst variance analysis. *Biophys. J.* **100**, 1568–1577 (2011).
88. Tomov, T. E. et al. Disentangling subpopulations in single-molecule FRET and ALEX experiments with photon distribution analysis. *Biophys. J.* **102**, 1163–1173 (2012).
89. Kalinin, S., Valeri, A., Antonik, M., Felekyan, S. & Seidel, C. A. Detection of structural dynamics by FRET: a photon distribution and fluorescence lifetime analysis of systems with multiple states. *J. Phys. Chem. B* **114**, 7983–7995 (2010).
90. Chung, H. S. & Eaton, W. A. Protein folding transition path times from single molecule FRET. *Curr. Opin. Struct. Biol.* **48**, 30–39 (2018).
91. Pirchi, M. et al. Photon-by-photon hidden Markov model analysis for microsecond single-molecule FRET kinetics. *J. Phys. Chem. B* **120**, 13065–13075 (2016).
92. Keller, B. G., Kobitski, A., Jaschke, A., Nienhaus, G. U. & Noe, F. Complex RNA folding kinetics revealed by single-molecule FRET and hidden Markov models. *J. Am. Chem. Soc.* **136**, 4534–4543 (2014).
93. Felekyan, S., Sanabria, H., Kalinin, S., Kuhnemuth, R. & Seidel, C. A. Analyzing Forster resonance energy transfer with fluctuation algorithms. *Methods Enzymol.* **519**, 39–85 (2013).
94. Gurunathan, K. & Levitus, M. FRET fluctuation spectroscopy of diffusing biopolymers: contributions of conformational dynamics and translational diffusion. *J. Phys. Chem. B* **114**, 980–986 (2010).

95. Schuler, B. Perspective: chain dynamics of unfolded and intrinsically disordered proteins from nanosecond fluorescence correlation spectroscopy combined with single-molecule FRET. *J. Chem. Phys.* **149**, 010901 (2018).
96. Nettels, D., Gopich, I. V., Hoffmann, A. & Schuler, B. Ultrafast dynamics of protein collapse from single-molecule photon statistics. *Proc. Natl Acad. Sci. USA* **104**, 2655–2660 (2007).
97. Yoo, J., Kim, J. Y., Louis, J. M., Gopich, I. V. & Chung, H. S. Fast three-color single-molecule FRET using statistical inference. *Nat. Commun.* **11**, 3336 (2020).
98. Ingargiola, A. et al. Multispot single-molecule FRET: high-throughput analysis of freely diffusing molecules. *PLoS ONE* **12**, e0175766 (2017).
99. Ingargiola, A., Weiss, S. & Lerner, E. Monte Carlo diffusion-enhanced photon inference: distance distributions and conformational dynamics in single-molecule FRET. *J. Phys. Chem. B* **122**, 11598–11615 (2018).
100. Nagy, P. et al. rFRET: a comprehensive, MATLAB-based program for analyzing intensity-based ratiometric microscopic FRET experiments. *Cytometry A* **89**, 376–384 (2016).
101. Widengren, J. et al. Single-molecule detection and identification of multiple species by multiparameter fluorescence detection. *Anal. Chem.* **78**, 2039–2050 (2006).
102. Lee, N. K. et al. Accurate FRET measurements within single diffusing biomolecules using alternating-laser excitation. *Biophys. J.* **88**, 2939–2953 (2005).
103. Margeat, E. et al. Direct observation of abortive initiation and promoter escape within single immobilized transcription complexes. *Biophys. J.* **90**, 1419–1431 (2006).
104. Frank, J. & Gonzalez, R. L. Jr Structure and dynamics of a processive Brownian motor: the translating ribosome. *Annu. Rev. Biochem.* **79**, 381–412 (2010).
105. Fan, J., Moreno, A. T., Baier, A. S., Loparo, J. J. & Peterson, C. L. H2A.Z deposition by SWR1C involves multiple ATP-dependent steps. *Nat. Commun.* **13**, 7052 (2022).
106. Gamarra, N., Johnson, S. L., Trnka, M. J., Burlingame, A. L. & Narlikar, G. J. The nucleosomal acidic patch relieves auto-inhibition by the ISWI remodeler SNF2h. *eLife* **7**, e35322 (2018).
107. Evans, G. W., Craggs, T. & Kapanidis, A. N. The rate-limiting step of DNA synthesis by DNA polymerase occurs in the fingers-closed conformation. *J. Mol. Biol.* **434**, 167410 (2022).
108. Berezhna, S. Y., Gill, J. P., Lamichhane, R. & Millar, D. P. Single-molecule Forster resonance energy transfer reveals an innate fidelity checkpoint in DNA polymerase I. *J. Am. Chem. Soc.* **134**, 11261–11268 (2012).
109. Lee, D., Oh, S., Cho, H., Yoo, J. & Lee, G. Mechanistic decoupling of exonuclease III multifunctionality into AP endonuclease and exonuclease activities at the single-residue level. *Nucleic Acids Res.* **50**, 2211–2222 (2022).
110. Reid, D. A. et al. Organization and dynamics of the nonhomologous end-joining machinery during DNA double-strand break repair. *Proc. Natl Acad. Sci. USA* **112**, E2575–E2584 (2015).
111. Singh, D., Sternberg, S. H., Fei, J., Doudna, J. A. & Ha, T. Real-time observation of DNA recognition and rejection by the RNA-guided endonuclease Cas9. *Nat. Commun.* **7**, 12778 (2016).
112. Yang, M. et al. The conformational dynamics of Cas9 governing DNA cleavage are revealed by single-molecule FRET. *Cell Rep.* **22**, 372–382 (2018).
113. Osuka, S. et al. Real-time observation of flexible domain movements in CRISPR–Cas9. *EMBO J.* **37**, e96941 (2018).
114. Chen, J. S. et al. Enhanced proofreading governs CRISPR–Cas9 targeting accuracy. *Nature* **550**, 407–410 (2017).
115. Chakraborty, A. et al. Opening and closing of the bacterial RNA polymerase clamp. *Science* **337**, 591–595 (2012).
116. Song, E. et al. Rho-dependent transcription termination proceeds via three routes. *Nat. Commun.* **13**, 1663 (2022).
117. Abelson, J. et al. Conformational dynamics of single pre-mRNA molecules during in vitro splicing. *Nat. Struct. Mol. Biol.* **17**, 504–512 (2010).
118. Rodgers, M. L. et al. Conformational dynamics of stem II of the U2 snRNA. *RNA* **22**, 225–236 (2016).
119. Roca, J., Santiago-Frangos, A. & Woodson, S. A. Diversity of bacterial small RNAs drives competitive strategies for a mutual chaperone. *Nat. Commun.* **13**, 2449 (2022).
120. Chandradoss, S. D., Schirle, N. T., Szczepaniak, M., MacRae, I. J. & Joo, C. A dynamic search process underlies microRNA targeting. *Cell* **162**, 96–107 (2015).
121. Fei, J., Kosuri, P., MacDougall, D. D. & Gonzalez, R. L. Jr. Coupling of ribosomal L1 stalk and tRNA dynamics during translation elongation. *Mol. Cell* **30**, 348–359 (2008).
122. Lapointe, C. P. et al. eIF5B and eIF1A reorient initiator tRNA to allow ribosomal subunit joining. *Nature* **607**, 185–190 (2022).
123. Ray, K. K. et al. Entropic control of the free-energy landscape of an archetypal biomolecular machine. *Proc. Natl Acad. Sci. USA* **120**, e2220591120 (2023).
124. Mazal, H., Iljina, M., Riven, I. & Haran, G. Ultrafast pore-loop dynamics in a AAA+ machine point to a Brownian-ratchet mechanism for protein translocation. *Sci. Adv.* **7**, eabg4674 (2021).
125. Zhuang, X. et al. Correlating structural dynamics and function in single ribozyme molecules. *Science* **296**, 1473–1476 (2002).
126. Liao, T. W. et al. Linking folding dynamics and function of SAM/SAH riboswitches at the single molecule level. *Nucleic Acids Res.* **51**, 8957–8969 (2023).
127. Schuler, B., Lipman, E. A. & Eaton, W. A. Probing the free-energy surface for protein folding with single-molecule fluorescence spectroscopy. *Nature* **419**, 743–747 (2002).
128. Kim, J. Y. & Chung, H. S. Disordered proteins follow diverse transition paths as they fold and bind to a partner. *Science* **368**, 1253–1257 (2020).
129. Zamel, J. et al. Structural and dynamic insights into α-synuclein dimer conformations. *Structure* **31**, 411–423.e6 (2023).
130. Galvanetto, N. et al. Extreme dynamics in a biomolecular condensate. *Nature* **619**, 876–883 (2023).
131. Okafor, I. C. & Ha, T. Single molecule FRET analysis of CRISPR–Cas9 single guide RNA folding dynamics. *J. Phys. Chem. B* **127**, 45–51 (2022).
132. Trucks, S., Hanspach, G. & Hengesbach, M. Eukaryote specific RNA and protein features facilitate assembly and catalysis of H/ACA snoRNPs. *Nucleic Acids Res.* **49**, 4629–4642 (2021).
133. Kim, H. et al. Protein-guided RNA dynamics during early ribosome assembly. *Nature* **506**, 334–338 (2014).
134. Duss, O. et al. Real-time assembly of ribonucleoprotein complexes on nascent RNA transcripts. *Nat. Commun.* **9**, 5087 (2018).
135. Marzano, N. R., Paudel, B. P., van Oijen, A. M. & Ecroyd, H. Real-time single-molecule observation of chaperone-assisted protein folding. *Sci. Adv.* **8**, eadd0922 (2022).
136. Chamachi, N. et al. Chaperones Skp and SurA dynamically expand unfolded OmpX and synergistically disassemble oligomeric aggregates. *Proc. Natl Acad. Sci. USA* **119**, e2118919119 (2022).
137. Dahiya, V. et al. Coordinated conformational processing of the tumor suppressor protein p53 by the Hsp70 and Hsp90 chaperone machineries. *Mol. Cell* **74**, 816–830.e7 (2019).
138. Schmid, S. & Hugel, T. Controlling protein function by fine-tuning conformational flexibility. *eLife* **9**, e57180 (2020).
139. Levring, J. et al. CFTR function, pathology and pharmacology at single-molecule resolution. *Nature* **616**, 606–614 (2023).
140. Han, S. et al. Cholesterol inhibits human voltage-gated proton channel hHv1. *Proc. Natl Acad. Sci. USA* **119**, e2205420119 (2022).
141. Wang, S., Vafabakhsh, R., Borschel, W. F., Ha, T. & Nichols, C. G. Structural dynamics of potassium-channel gating revealed by single-molecule FRET. *Nat. Struct. Mol. Biol.* **23**, 31–36 (2016).
142. Zhao, Y. et al. Substrate-modulated gating dynamics in a Na^+-coupled neurotransmitter transporter homologue. *Nature* **474**, 109–113 (2011).
143. Ciftci, D. et al. Linking function to global and local dynamics in an elevator-type transporter. *Proc. Natl Acad. Sci. USA* **118**, e2025520118 (2021).
144. Zhu, L. et al. Realtime observation of ATP-driven single B12 molecule translocation through BtuCD-F. Preprint at *bioRxiv* https://doi.org/10.1101/2022.12.02.518935 (2022).
145. Vafabakhsh, R., Levitz, J. & Isacoff, E. Y. Conformational dynamics of a class C G-protein-coupled receptor. *Nature* **524**, 497–501 (2015).
146. Liu, T., Khanal, S., Hertslet, G. D. & Lamichhane, R. Single-molecule analysis reveals that a glucagon-bound extracellular domain of the glucagon receptor is dynamic. *J. Biol. Chem.* **299**, 105160 (2023).
147. Heng, J. et al. Function and dynamics of the intrinsically disordered carboxyl terminus of β_2-adrenergic receptor. *Nat. Commun.* **14**, 2005 (2023).
148. Liauw, B. W., Afsari, H. S. & Vafabakhsh, R. Conformational rearrangement during activation of a metabotropic glutamate receptor. *Nat. Chem. Biol.* **17**, 291–297 (2021).
149. Lecat-Guillet, N. et al. Concerted conformational changes control metabotropic glutamate receptor activity. *Sci. Adv.* **9**, eadf1378 (2023).
150. Landes, C. F., Rambhadran, A., Taylor, J. N., Salatan, F. & Jayaraman, V. Structural landscape of isolated agonist-binding domains from single AMPA receptors. *Nat. Chem. Biol.* **7**, 168–173 (2011).
151. Asher, W. B. et al. GPCR-mediated β-arrestin activation deconvoluted with single-molecule precision. *Cell* **185**, 1661–1675.e16 (2022).
152. Diaz-Salinas, M. A. et al. Conformational dynamics and allosteric modulation of the SARS-CoV-2 spike. *eLife* **11**, e75433 (2022).
153. Munro, J. B. et al. Conformational dynamics of single HIV-1 envelope trimers on the surface of native virions. *Science* **346**, 759–763 (2014).
154. Ngo, T. T., Zhang, Q., Zhou, R., Yodh, J. G. & Ha, T. Asymmetric unwrapping of nucleosomes under tension directed by DNA local flexibility. *Cell* **160**, 1135–1144 (2015).
155. Ngo, T. T. M. et al. Dependence of nucleosome mechanical stability on DNA mismatches and histone variants. Preprint at *bioRxiv* https://doi.org/10.1101/2022.11.21.517409 (2022).
156. Berman, H. M. et al. The Protein Data Bank. *Nucleic Acids Res.* **28**, 235–242 (2000).
157. Jumper, J. et al. Highly accurate protein structure prediction with AlphaFold. *Nature* **596**, 583–589 (2021).
158. Gotz, M. et al. A blind benchmark of analysis tools to infer kinetic rate constants from single-molecule FRET trajectories. *Nat. Commun.* **13**, 5402 (2022).
159. Agam, G. et al. Reliability and accuracy of single-molecule FRET studies for characterization of structural dynamics and distances in proteins. *Nat. Methods* **20**, 523–535 (2023).
160. Martens, K. J. A. et al. Visualisation of dCas9 target search in vivo using an open-microscopy framework. *Nat. Commun.* **10**, 3552 (2019).
161. Ambrose, B. et al. The smfBox is an open-source platform for single-molecule FRET. *Nat. Commun.* **11**, 5641 (2020).
162. Rueden, C. T. et al. ImageJ2: imageJ for the next generation of scientific image data. *BMC Bioinformatics* **18**, 529 (2017).
163. Greenfeld, M. et al. Single-molecule dataset (SMD): a generalized storage format for raw and processed single-molecule data. *BMC Bioinformatics* **16**, 3 (2015).

164. Vallat, B., Webb, B., Westbrook, J. D., Sali, A. & Berman, H. M. Development of a prototype system for archiving integrative/hybrid structure models of biological macromolecules. *Structure* **26**, 894–904.e2 (2018).
165. Rasnik, I., McKinney, S. A. & Ha, T. Nonblinking and long-lasting single-molecule fluorescence imaging. *Nat. Methods* **3**, 891–893 (2006).
166. Bates, M., Blosser, T. R. & Zhuang, X. Short-range spectroscopic ruler based on a single-molecule optical switch. *Phys. Rev. Lett.* **94**, 108101 (2005).
167. Arseni, C. et al. Time-related variations of some biochemical parameters in patients with short- or long-lasting post-traumatic coma. *Rom. J. Neurol. Psychiatry* **28**, 209–223 (1990).
168. Dagdas, Y. S., Chen, J. S., Sternberg, S. H., Doudna, J. A. & Yildiz, A. A conformational checkpoint between DNA binding and cleavage by CRISPR–Cas9. *Sci. Adv.* **3**, eaao0027 (2017).
169. Wang, Y. et al. Real-time observation of Cas9 postcatalytic domain motions. *Proc. Natl Acad. Sci. USA* **118**, e2010650118 (2021).
170. Grimm, J. B. et al. A general method to improve fluorophores using deuterated auxochromes. *JACS Au* **1**, 690–696 (2021).
171. Kim, J. M. et al. Dynamic 1D search and processive nucleosome translocations by RSC and ISW2 chromatin remodelers. Preprint at *bioRxiv* https://doi.org/10.1101/2023.06.13.544671 (2023).
172. Lang, M. J., Fordyce, P. M., Engh, A. M., Neuman, K. C. & Block, S. M. Simultaneous, coincident optical trapping and single-molecule fluorescence. *Nat. Methods* **1**, 133–139 (2004).
173. Gebhardt, C. et al. Labelizer: systematic selection of protein residues for covalent fluorophore labeling. Preprint at *bioRxiv* https://doi.org/10.1101/2023.06.12.544586 (2023).
174. Shi, X., Lim, J. & Ha, T. Acidification of the oxygen scavenging system in single-molecule fluorescence studies: in situ sensing with a ratiometric dual-emission probe. *Anal. Chem.* **82**, 6132–6138 (2010).
175. Okumus, B., Wilson, T. J., Lilley, D. M. & Ha, T. Vesicle encapsulation studies reveal that single molecule ribozyme heterogeneities are intrinsic. *Biophys. J.* **87**, 2798–2806 (2004).
176. Chung, H. S. et al. Extracting rate coefficients from single-molecule photon trajectories and FRET efficiency histograms for a fast-folding protein. *J. Phys. Chem. A* **115**, 3642–3656 (2011).
177. Chen, J. et al. High-throughput platform for real-time monitoring of biological processes by multicolor single-molecule fluorescence. *Proc. Natl Acad. Sci. USA* **111**, 664–669 (2014).
178. Cisse, I. I., Kim, H. & Ha, T. A rule of seven in Watson–Crick base-pairing of mismatched sequences. *Nat. Struct. Mol. Biol.* **19**, 623–627 (2012).
179. Sanabria, H. et al. Resolving dynamics and function of transient states in single enzyme molecules. *Nat. Commun.* **11**, 1231 (2020).
180. Hellenkamp, B., Wortmann, P., Kandzia, F., Zacharias, M. & Hugel, T. Multidomain structure and correlated dynamics determined by self-consistent FRET networks. *Nat. Methods* **14**, 174–180 (2017).
181. Soranno, A. et al. Integrated view of internal friction in unfolded proteins from single-molecule FRET, contact quenching, theory, and simulations. *Proc. Natl Acad. Sci. USA* **114**, E1833–E1839 (2017).
182. Chen, J. et al. The structural heterogeneity of α-synuclein is governed by several distinct subpopulations with interconversion times slower than milliseconds. *Structure* **29**, 1048–1064.e6 (2021).
183. Trofymchuk, K. et al. Addressable nanoantennas with cleared hotspots for single-molecule detection on a portable smartphone microscope. *Nat. Commun.* **12**, 950 (2021).
184. Holzmeister, P., Acuna, G. P., Grohmann, D. & Tinnefeld, P. Breaking the concentration limit of optical single-molecule detection. *Chem. Soc. Rev.* **43**, 1014–1028 (2014).
185. Jain, A. et al. Probing cellular protein complexes using single-molecule pull-down. *Nature* **473**, 484–488 (2011).
186. Mao, C. P. et al. Protein detection in blood with single-molecule imaging. *Sci Adv* **7**, eabg6522 (2021).
187. Hartmann, A. et al. An automated single-molecule FRET platform for high-content, multiwell plate screening of biomolecular conformations and dynamics. *Nat. Commun.* **14**, 6511 (2023).
188. Severins, I., Joo, C. & van Noort, J. Exploring molecular biology in sequence space: the road to next-generation single-molecule biophysics. *Mol. Cell* **82**, 1788–1805 (2022).
189. Pati, A. K. et al. Tuning the Baird aromatic triplet-state energy of cyclooctatetraene to maximize the self-healing mechanism in organic fluorophores. *Proc. Natl Acad. Sci. USA* **117**, 24305–24315 (2020).
190. Isselstein, M. et al. Self-healing dyes—keeping the promise? *J. Phys. Chem. Lett.* **11**, 4462–4480 (2020).
191. Zhang, Y. et al. General strategy to improve the photon budget of thiol-conjugated cyanine dyes. *J. Am. Chem. Soc.* https://doi.org/10.1021/jacs.2c12635 (2023).
192. Sow, M. et al. High-throughput nitrogen-vacancy center imaging for nanodiamond photophysical characterization and pH nanosensing. *Nanoscale* **12**, 21821–21831 (2020).
193. Glushkov, E. et al. Engineering optically active defects in hexagonal boron nitride using focused ion beam and water. *ACS Nano* **16**, 3695–3703 (2022).
194. Vermeer, B. & Schmid, S. Can DyeCycling break the photobleaching limit in single-molecule FRET? *Nano Res.* **15**, 9818–9830 (2022).
195. Kummerlin, M., Mazumder, A. & Kapanidis, A. N. Bleaching-resistant, near-continuous single-molecule fluorescence and FRET based on fluorogenic and transient DNA binding. *Chemphyschem* **24**, e202300175 (2023).
196. Sharonov, A. & Hochstrasser, R. M. Wide-field subdiffraction imaging by accumulated binding of diffusing probes. *Proc. Natl Acad. Sci. USA* **103**, 18911–18916 (2006).
197. Albitz, E. et al. Bioorthogonal ligation-activated fluorogenic FRET dyads. *Angew. Chem. Int. Ed.* **61**, e202111855 (2022).
198. Ploetz, E. et al. Forster resonance energy transfer and protein-induced fluorescence enhancement as synergetic multi-scale molecular rulers. *Sci. Rep.* **6**, 33257 (2016).
199. Qiu, Y. et al. Srs2 prevents Rad51 filament formation by repetitive motion on DNA. *Nat. Commun.* **4**, 2281 (2013).
200. Schubert, J., Schulze, A., Prodromou, C. & Neuweiler, H. Two-colour single-molecule photoinduced electron transfer fluorescence imaging microscopy of chaperone dynamics. *Nat. Commun.* **12**, 6964 (2021).
201. Schmid, S., Stommer, P., Dietz, H. & Dekker, C. Nanopore electro-osmotic trap for the label-free study of single proteins and their conformations. *Nat. Nanotechnol.* **16**, 1244–1250 (2021).
202. Tang, L. et al. Combined quantum tunnelling and dielectrophoretic trapping for molecular analysis at ultra-low analyte concentrations. *Nat. Commun.* **12**, 913 (2021).
203. Gordon, R. Future prospects for biomolecular trapping with nanostructured metals. *ACS Photonics* **9**, 1127–1135 (2022).
204. Hou, S., Exell, J. & Welsher, K. Real-time 3D single molecule tracking. *Nat. Commun.* **11**, 3607 (2020).
205. Dyla, M. et al. Dynamics of P-type ATPase transport revealed by single-molecule FRET. *Nature* **551**, 346–351 (2017).
206. Zhang, J. et al. Specific structural elements of the T-box riboswitch drive the two-step binding of the tRNA ligand. *eLife* **7**, e39518 (2018).
207. Hildebrandt, L. L., Preus, S. & Birkedal, V. Quantitative single molecule FRET efficiencies using TIRF microscopy. *Faraday Discuss.* **184**, 131–142 (2015).

Acknowledgements

The authors thank the National Institutes of Health (NIH) for funding (R35 GM 122569 to T.H.) and the National Research Foundation of Korea (NRF-2023R1A2C2006606 to N.K.L.). T.H. is an investigator with the Howard Hughes Medical Institute.

Author contributions

Introduction (T.H.); Experimentation (T.H., N.K.L. and S.Y.); Results (T.H., J.F. and S.P.); Applications (T.H. and R.L.G.); Reproducibility and data deposition (T.H. and S.S.); Limitations and optimizations (T.H.); Outlook (T.H. and S.S.); Overview of the Primer (T.H.).

Competing interests

The authors declare no competing interests.

Additional information

Peer review information *Nature Reviews Methods Primers* thanks the anonymous reviewer(s) for their contribution to the peer review of this work.

Publisher's note Springer Nature remains neutral with regard to jurisdictional claims in published maps and institutional affiliations.

Related links

µManager: https://micro-manager.org
Single: https://github.com/pjb7687/single
smCamera: https://github.com/Ha-SingleMoleculeLab/smCamera2